A comparison of mercaptothiazoline, mercaptobenzothiazole, mercaptobenzimidazole, and mercaptobenzoxazole as inhibitors of 90/10 cupro-nickel alloy corrosion in seawater
by Jonathan Paul Storvick

A thesis submitted in partial fulfillment of the requirements for the degree of Doctor of Philosophy in Chemistry
Montana State University


Abstract:
The corrosion resistance of 90/10 cupro-nickel alloy in seawater is due to the formation of a protective cuprous oxide layer. This corrosion resistance can be improved through the application of inhibitors. The purpose of this investigation was to study the action of 2-mercaptothiazoline (MT), 2-mercaptobenzo-thiazole (MBT), 2-mercaptobenzimidazole (MBI), and 2-mercapto-benzoxazole (MBO) as inhibitors of 90/10 cupro-nickel alloy corrosion in seawater.

A pretreatment procedure was outlined to ensure that experimental results were representative of the alloy and reproducible. Material balance techniques in conjunction with scanning auger microscopy were utilized to study the corrosion processes. A set of base conditions was established and used as a starting point for parameter variation. The individual effects of exposure time, temperature, salinity, and dissolved oxygen were studied to determine a mechanism for the corrosion. During initial exposure the diffusion of OH- ions generated by the cathodic reduction of O2 is likely to be rate limiting. After prolonged exposure the growth rate of oxide is limited by diffusion of cations to the solid-solution interface.

Inhibition of the corrosion was studied with 10-3 M and 10-4M inhibitor concentrations in the seawater. Pretreatment of the surface via immersion in 60°C aqueous solutions of the inhibitors for two minutes was also investigated. The observed order of inhibition efficiency, MBT > MBI = MBO > MT, is explained in terms of a theory of chemisorptive inhibition. Water-insoluble thin polymeric films are formed by a surface reaction between cuprous ions and adsorbed inhibitor molecules via a discharge and nucleation mechanism. The resultant film acts as a barrier to corrosive environments.

# A COMPARISON OF MERCAPTOTHIAZOLINE, MERCAPTOBENZOTHIAZOLE, MERCAPTOBENZIMIDAZOLE, AND MERCAPTOBENZOXAZOLE AS INHIBITORS OF 90/10 CUPRO-NICKEL ALLOY CORROSION IN SEAWATER

by

Jonathan Paul Storvick

A thesis submitted in partial fulfillment
of the requirements for the degree

of

Doctor of Philosophy

in

Chemistry

Montana State University
Bozeman, Montana

May 1986

APPROVAL

of a thesis submitted by

Jonathan Paul Storvick

This thesis has been read by each member of the thesis committee and has been found to be satisfactory regarding content, English usage, format, citations, bibliographic style, and consistency, and is ready for submission to the College of Graduate Studies.

5/16/86
Date

Gordon Pagenkopf
Chairperson, Graduate committee

Approved for the Major Department

5/16/86
Date

Edwin H. Abbott
Head, Major Department

Approved for the College of Graduate Studies

5/28/86
Date

Henry L Parsons
Graduate Dean

STATEMENT OF PERMISSION TO USE

In presenting this thesis in partial fulfillment of the requirements for a doctoral degree at Montana State University, I agree that the Library shall make it available to borrowers under rules of the library. I further agree that copying of this thesis is allowable only for scholarly purposes, consistent with "fair use" as prescribed in the U.S. Copyright Law. Requests for extensive copying or reproduction of this thesis should be referred to the University Microfilms International, 300 North Zeeb Road, Ann Arbor, Michigan, 48106, to whom I have granted "the exclusive right to reproduce and distribute copies of the dissertation in and from microfilm and the right to reproduce and distribute by abstract in any format."

Signature Jonathan P. Stovall

Date 5/16/86

ACKNOWLEDGMENT

I am very grateful to Dr. Gordon Pagenkopf for his guidance and support throughout the course of my graduate studies. I am also grateful to the faculty of the Chemistry Department and the staff of the CRISS facility for their assistance with this project. Finally, a special thanks to Dave Dobb for his helpful suggestions and ideas, and to all other members of our research group from whom I have learned much.

TABLE OF CONTENTS

TABLE OF CONTENTS (continued)

# LIST OF TABLES

# LIST OF FIGURES

LIST OF FIGURES (continued)

LIST OF FIGURES (continued)

LIST OF FIGURES (continued)

## ABSTRACT

The corrosion resistance of 90/10 cupro-nickel alloy in seawater is due to the formation of a protective cuprous oxide layer. This corrosion resistance can be improved through the application of inhibitors. The purpose of this investigation was to study the action of 2-mercaptothiazoline (MT), 2-mercaptobenzothiazole (MBT), 2-mercaptobenzimidazole (MBI), and 2-mercaptobenzoxazole (MBO) as inhibitors of 90/10 cupro-nickel alloy corrosion in seawater.

A pretreatment procedure was outlined to ensure that experimental results were representative of the alloy and reproducible. Material balance techniques in conjunction with scanning auger microscopy were utilized to study the corrosion processes. A set of base conditions was established and used as a starting point for parameter variation. The individual effects of exposure time, temperature, salinity, and dissolved oxygen were studied to determine a mechanism for the corrosion. During initial exposure the diffusion of $OH^-$ ions generated by the cathodic reduction of $O_2$ is likely to be rate limiting. After prolonged exposure the growth rate of oxide is limited by diffusion of cations to the solid-solution interface.

Inhibition of the corrosion was studied with $10^{-3}$ M and $10^{-4}$ M inhibitor concentrations in the seawater. Pretreatment of the surface via immersion in 60°C aqueous solutions of the inhibitors for two minutes was also investigated. The observed order of inhibition efficiency, MBT > MBI $\cong$ MBO > MT, is explained in terms of a theory of chemisorptive inhibition. Water-insoluble thin polymeric films are formed by a surface reaction between cuprous ions and adsorbed inhibitor molecules via a discharge and nucleation mechanism. The resultant film acts as a barrier to corrosive environments.

# INTRODUCTION

## Copper-Nickel Alloys: Uses, Corrosion Behavior, and Protective Layer Formation

The cost of corrosion and protection against corrosion in the United States has been estimated at eight billion dollars per year[1]. Although this is a very large cost, it is not surprising when considering corrosion occurs whenever metals and other materials are used. Corrosion is inevitable, but in many cases its cost can be reduced, and catastrophic failure may be prevented.

Corrosion may be defined as the destruction or deterioration of a material due to its reaction with the environment other than by mechanical means. This study is concerned with the oxidation of 90/10 cupro-nickel alloy due to exposure to seawater.

Copper and copper alloys are employed extensively for fresh water and marine applications. The main reasons for these uses include (a) excellent corrosion and biofouling resistance, (b) good mechanical workability, (c) galvanic compatibility with other copper alloy system components, (d) reliability and economy. Applications for copper alloys include condensor tubing, ocean thermal energy conversion heat exchangers, and piping systems for offshore seawater platforms[2,3].

A problem commonly encountered in conjunction with corrosion is fouling. Two major problems associated with fouling are lowered heat transfer capability and inhibited flow of liquids through

pipes. The best way to prevent fouling is to choose an alloy which is resistant, like cupro-nickel alloys. Fouling resistance is primarily due to release of cupric ions during corrosion. These cupric ions are toxic to marine organisms attaching to the metal surface[4]. Although resistant organisms may colonize, a buildup of non-protective corrosion products such as paratacamite ($Cu_2(OH)_3Cl$) between the organisms and the metal surface will allow the organisms to be swept away[5].

The long-term, steady-state corrosion rate of 90/10 cupro-nickel has been shown to be less than 0.5 mils per year[3]. One result of the excellent corrosion and fouling resistance is a reduction in the required pipe thickness and diameter for many applications.

Corrosion resistance of copper alloys is primarily due to the formation of a surface oxide film acting as a barrier between the metal and the environment. Copper dissolves anodically in aqueous environments forming the divalent $Cu^{2+}$. The equilibrium relation

$$2\ Cu^{+} \rightleftarrows Cu + Cu^{2+} \qquad (1)$$

is displaced far to the right ($K = 1.7 \times 10^6$). However, if complexes are formed, as between $Cu^{+}$ and $Cl^{-}$ in a chloride solution, the depletion of $Cu^{+}$ to $CuCl_2^{-}$ favors $Cu^{+}$ as the major dissolution product. Hence the oxide film formed is principally composed of $Cu_2O$.[6] The film may also contain alloying metals in the oxide lattice, giving the film its corrosion resistant properties.

Cupro-nickel alloys are resistant to corrosion in many applications, due to doping of the $Cu_2O$ lattice with $Ni^{2+}$ ions.

This doping lowers the electrical and ionic conductivity of the protective film, rendering it more inert to electrochemical activity.

Other metals are added to the alloy to improve mechanical properties and/or to increase corrosion resistance. Iron is added to enhance corrosion resistance in seawater. The lowest corrosion rates without iron additions are at the 25 at 30% nickel level, whereas with iron these rates are achieved at a 10% nickel level[7]. The effect is an enhancement of nickel incorporation into the $Cu_2O$ lattice. The metal reactivity is related to chemisorbed oxygen films, which are favored by electron vacancies in the metal. These adsorbed oxygen films are not diffusion barriers, but act instead to decrease metal reaction kinetics by impeding metal ion hydration. Thus alloyed transition metals (Fe, Mn) added in small amounts, shift the critical Ni composition for passivity to lower values, as shown in Figure 1. This is explained by the electron configuration theory of passivity [8].

Fontana and Greene[1] classify corrosion by the forms in which it is displayed, based on the appearance of the corroded metal. These forms are described as (1) uniform, or general attack, (2) galvanic, or two-metal corrosion, (3) crevice corrosion, (4) pitting, (5) intergranular corrosion, (6) selective leaching, or parting, (7) erosion corrosion, and (8) stress corrosion. In most applications the primary reason for failure is localized rather than general attack, so uniform corrosion is not a problem. Copper-nickel alloy systems are galvanically compatible with other

copper alloy system components such as pumps and valves, so two-metal corrosion is generally not a problem either.

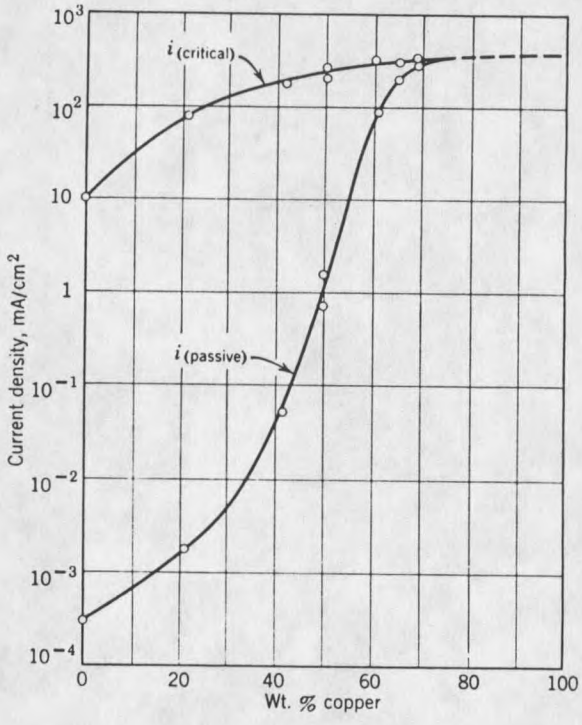


Figure 1. Critical and Passive Current Densities from Potentiostatic Anodic Polarization Curves for Copper-Nickel Alloys in 1 N $H_2SO_4$, 25°C.[8]

Crevice corrosion is usually associated with small volumes of stagnant solution in protected areas such as holes, crevices, gasket surfaces, lap joints, or under surface deposits. The crevice corrosion area must be wide enough to permit liquid entry, but small enough to maintain a stagnant zone. During the initial stages of corrosion the oxygen in the zone is depleted, while the surrounding metal has an adequate supply, thus the depleted region becomes anodic and corrodes more rapidly. Metal dissolution in the crevice produces cations which must be balanced by migration

of chloride ions into the crevice. The formation of soluble metal chlorides increases the metal dissolution rate, and through migration the result is a rapidly accelerating or auto-catalytic process.

Pitting is a form of extremely localized attack with holes in the metal as the end result. It is an autocatalytic process, whereby corrosion reactions within a pit produce conditions which stimulate continued growth. This process is shown in Figure 2. It is very similar to crevice corrosion in that the formation of soluble metal chlorides increases the metal dissolution rate, and an anodic current develops. Adjacent areas become cathodic resulting in the formation of an active-passive cell.

Copper-nickel alloys are not susceptible to intergranular corrosion, and selective leaching or dealloying is not a problem either as long as temperatures are kept low (<100°C).[2] Copper-zinc alloys do suffer from dealloying, however. The process is referred to as dezincification.

Erosion corrosion is an acceleration in the rate of deterioration due to the relative movement betwen a corrosive fluid and the metal surface. At high flow rates shear forces can strip off protective $Cu_2O$ layers and cause erosion corrosion or impingement damage. The more adherent and protective the passive film on an alloy, the greater its resistance will be to impingement or erosion corrosion. Copper-nickel alloys exhibit excellent corrosion resistance at low velocities, but are subject to erosion

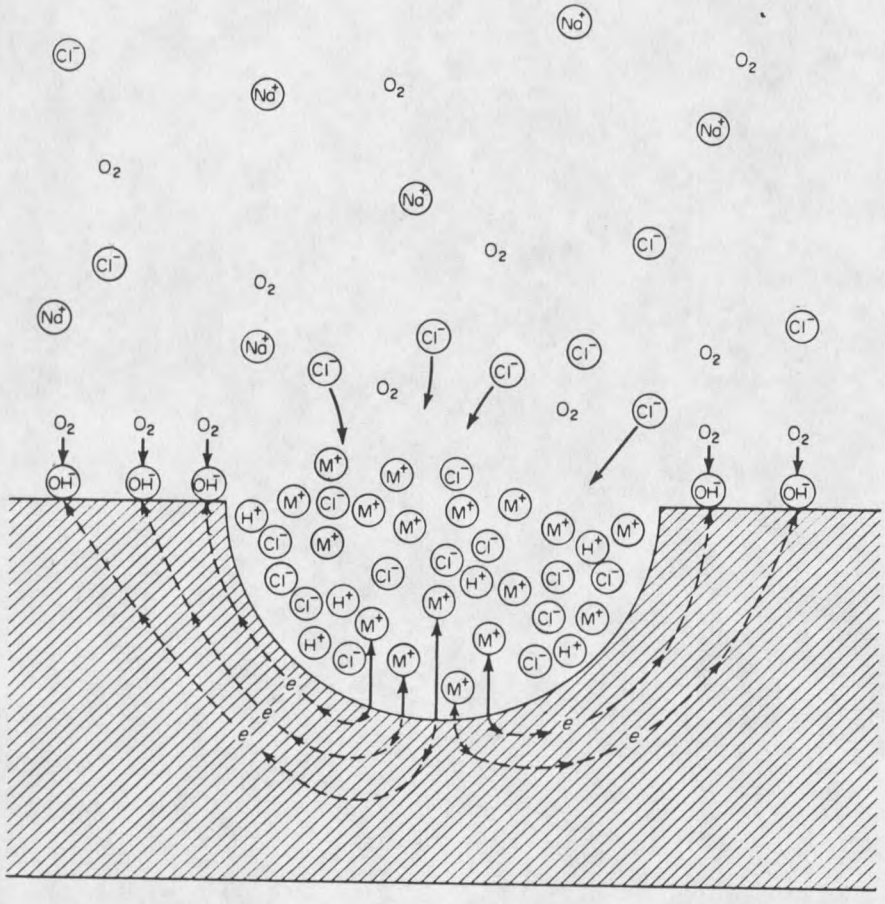


Figure 2. Autocatalytic Processes in a Corrosion Pit[1].

corrosion at higher flow rates. Other factors which affect erosion corrosion include pH, water temperature, oxygen content, gas bubbles, and silt particles in the corrosive medium[9].

Stress corrosion cracking occurs when a metal is placed in tensile stress in a corrosive environment. Important variables which affect this type of corrosion are temperature, solution composition, metal composition, stress, and metal structure. From outward appearance one might conclude brittle mechanical fracture was occuring, while local corrosion processes are actually

responsible. These cracks may form intergranularly or transgranularly, the most susceptible copper alloys are the brasses when exposed to ammonia or amines in the presence of oxygen and moisture[8]. Cupro-nickel alloys in condenser applications do not generally suffer stress corrosion cracking, as stresses are low and environmental conditions for cracking are not present.

The eight forms of corrosion have varying degrees of importance in the corrosion of cupro-nickel alloys in seawater. Some play an important role and some do not. Certain agressive ions and molecules such as $Cl^-$, $S^{2-}$ and $NH_3$ can be important in promoting corrosion of cupro-nickel alloys.

Chloride forms complex ions of the form $CuCl_x^{1-x}$ with cuprous ions and may accelerate metal loss. The mechanism has been described as follows:

$$Cu + Cl^- \longrightarrow CuCl(ads) + e^- \quad (2)$$

$$CuCl(ads) \longrightarrow CuCl \quad (3)$$

$$CuCl + Cl^- \longrightarrow CuCl_2^- \quad (4)$$

The kinetics are primarily governed by diffusion of cuprous complexes from the surface, the final step in this case is rate determining[10-13].

Copper-nickel alloys suffer accelerated corrosion in sulfide polluted seawater. The presence of dissolved sulfide interferes with the formation of a passive layer, as a porous cuprous sulfide film forms rather than a protective cuprous oxide layer. When oxygen is present the process is accelerated even further. The ionic and electrical conductivity is increased by $S^{2-}$ ions

incorporated into the oxide lattice, leading to lowered resistance to anodic reactions[14,15].

Sulfide is present in seawater as a result of decay in marine organisms and plants. The oxidation of organic material can lead to depletion of oxygen. Under these anaerobic conditions sulfate reducing bacteria can reduce sulfates to sulfides, thus increasing the corrosion rates.

Ammonia has been shown to attack copper and copper alloys, resulting in the formation of a soluble copper ammonia complex. The reaction of hydrated copper ions with ammonia is as follows:

$$Cu(H_2O)_x^{2+} + 4NH_3 \longrightarrow Cu(NH_3)_4^{2+} + XH_2O. \qquad (5)$$

Copper and its alloys are well suited for handling anhydrous ammonia solutions, but with water present this is not the case[2].

The corrosion product layer which forms when copper-nickel alloys corrode is $Cu_2O$, and is protective of the alloy against further corrosion. Although the $Cu_2O$ is a "passive" oxide it is not completely unreactive, and chloride ions in seawater continue to dissolve the oxide while new $Cu_2O$ is formed at the metal surface. The $Cu_2O$ reaches a protective thickness only after several days of exposure, and grows by a solid-state mechanism involving migration of cations through the oxide layer to react with adsorbed anions on the surface.

## Auger Spectroscopy

Auger Emission Spectroscopy (AES) was utilized in this study for analysis of corrosion products formed on the surface of the

alloy. This surface analytical technique provides several types of information including elemental concentrations, depth profiles, and scanning electron micrographs showing surface morphology. It is a truly surface analytical technique as the auger electrons detected usually originate within a surface volume ~30Å deep[16].

Surface analytical techniques such as Auger spectroscopy (AES), Electron Spectroscopy for Chemical Analysis (ESCA) or (XPS), and Secondary Ion Mass Spectroscopy (SIMS) have recently become popular in corrosion studies[17-22]. ESCA provides chemical state information while AES yields detailed chemical analysis with depth through ion milling. SIMS is a very sensitive technique for a number of elements; the sensitivity for one particular element depends very much on the composition of the sample however. Chemical information is also obtainable with SIMS. Auger Spectroscopy was selected for this study as quantitative analysis with depth was desired.

The AES technique for chemical analysis is based on the Auger radiationless process, shown in Figure 3. When a core level of a surface atom is ionized by the electron beam (1-10 KeV), the atom decays through an electronic rearrangement leaving the atom doubly ionized. The energy difference between the two states is imparted to the ejected auger electron, whose kinetic energy is characteristic of the parent atom. If the auger process occurs within several angstroms of the surface, the auger electrons may escape without loss of energy, giving rise to peaks in the secondary electron distribution. As there is a very large

secondary electron background, peaks are detected by computer differentiation of the energy distribution function, N(e).

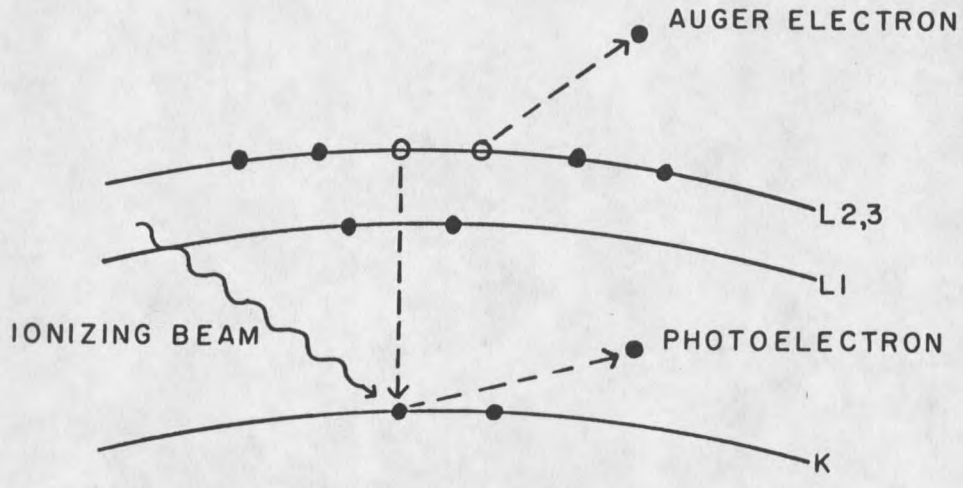


Figure 3. Electronic Origin of Auger Electrons.

The auger spectrometer consists of an ultra high vacuum system, an electron gun for sample excitation, an energy analyzer for detection of auger electron peaks, a TV monitor and storage scope for secondary electron imaging and micrographs, and a computer operated multichannel analyzer for data aquisition and storage. A schematic of the experimental arrangement used for obtaining auger spectra is shown in Figure 4. The sensitivity of the auger technique depends on the transition probability, the incident beam current and energy, and the collection efficiency of the cylindrical mirror analyzer (CMA). Detection limits are between 0.02 and 0.2 atomic percent, and all elements above helium produce auger peaks.

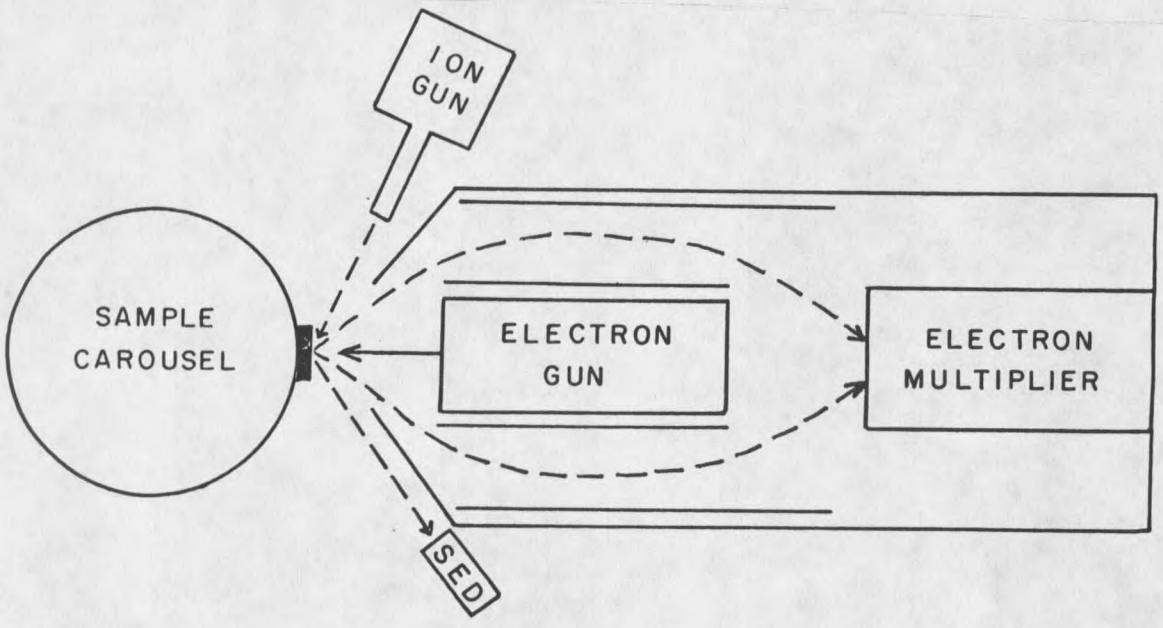


Figure 4. Schematic Diagram of AES Analytical System.

A typical auger spectra for 90/10 cupro-nickel alloy is shown in Figure 5. The N(e) spectra has been differentiated and smoothed. The survey shows the elemental surface composition of a sample corroded for two hours in 1/3 strength seawater, plotted as d(N(e))/dE versus kinetic energy.

The peak to peak heights in the differential spectrum may be utilized together with the sensitivity factors for the transition to obtain quantitative data, or atomic concentration percent. The relative auger sensitivity factors are shown in Figure 6. As there is a linear relationship between auger peak to peak amplitude and primary electron beam current, the sensitivity factors may be employed to calculate the atomic concentration with equation (6).

$$C_x = \frac{Px/Sx}{Pi/Si} \times 100 \qquad (6)$$

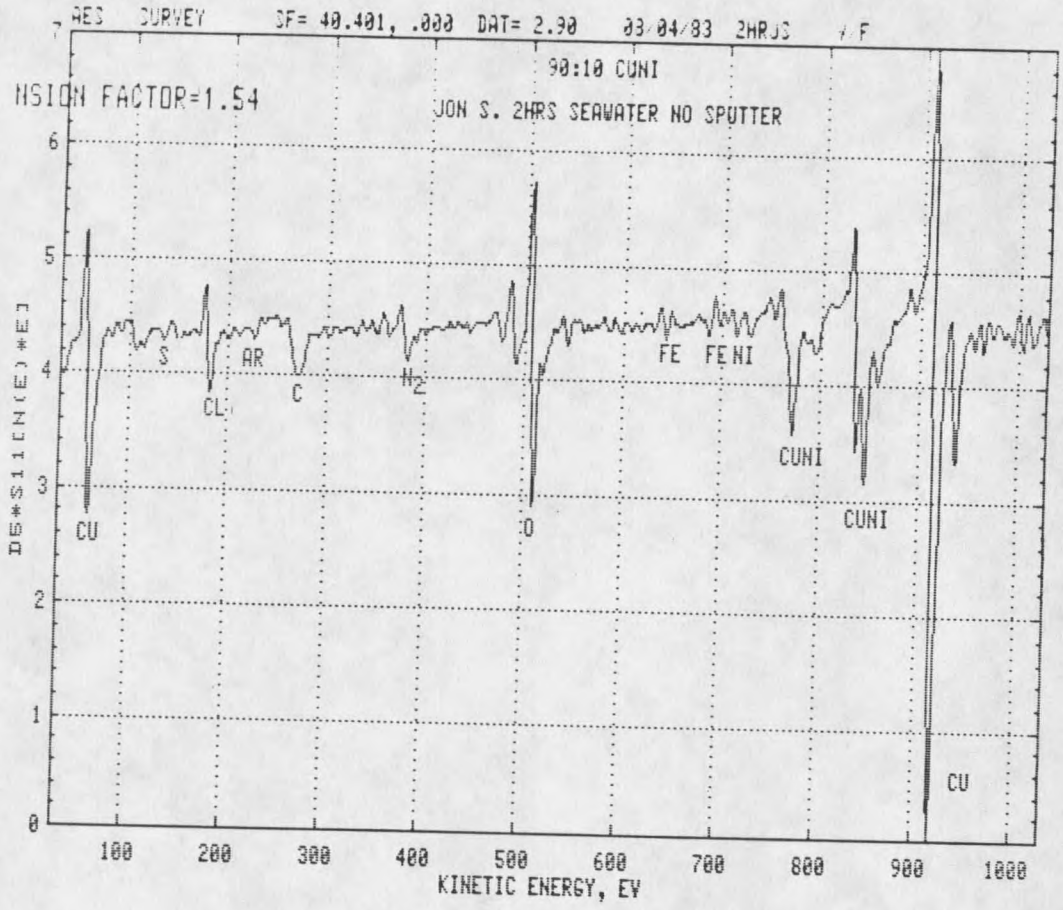


Figure 5. Auger General Survey of Coupon Corroded 2 Hours in 1/3 Strength Seawater.

In this equation $C_x$ is the concentration of element X, Px is the peak to peak height for the transition, and Sx is the relative sensitivity factor for element X. Pi and Si are the peak to peak heights and sensitivity factors for all i elements detected in the sample[16].

The most useful mode in which the scanning auger microprobe was used in this study was depth profiling. The ion gun (Figure 4) sputtered away the uppermost layer on the corroded alloy enabling data collection on subsurface layers. Argon ions were

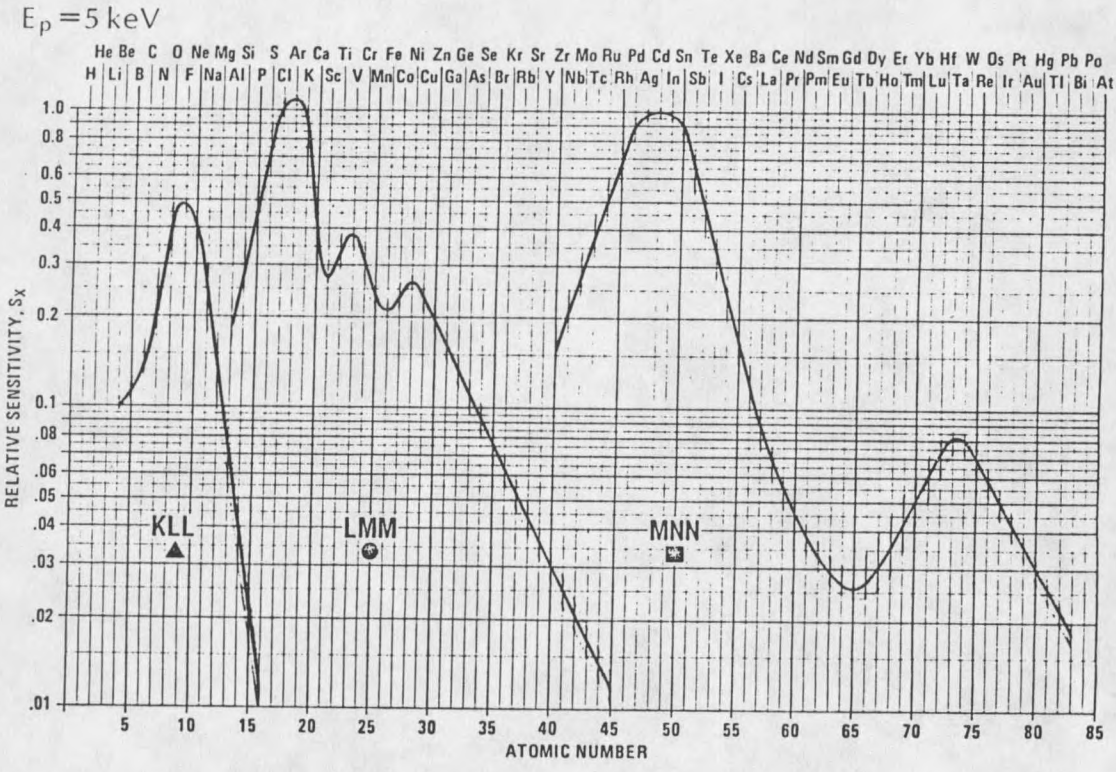


Figure 6. Relative Auger Sensitivites of the Elements[16].

accelerated to the surface and rastered over an area much larger than the area in which data is collected (where the electron beam is rastered). It was crucial to line up the two beams by means of a device called a faraday cup, so one could be sure data was taken from the center of the sputter crater. The rate of ion milling may be varied by means of a bleed valve controlling the quantity of argon let into the system, altering the accelerating voltage applied, and also by varying the area over which the ion beam is rastered.

With calibration the sputter time may be converted to depth, thus yielding more quantitative and useful data.

Several problems may be encountered while ion milling samples, including "knock on" effects, preferential sputtering, and sample damage. "Knocking on" may occur if the incident argon ions have sufficient energy to penetrate the surface and be retained. This will have the effect of diluting the surface concentration of the elements of interest, and may also disrupt the lattice by pushing surface metal atoms into underlying layers. This only occurs at high acceleration energies and can be avoided by using moderate etch rates.

Preferential sputtering is a situation in which one component in a sample is sputtered away faster than another component, resulting in concentration data which is non-representative of the sample. Researchers have reported this to be a problem with cupro-nickel alloys[23-25]. However, the results of this study showed no change in surface composition with sputtering on clean, uncorroded samples over long time periods (>1hr). The difference in results is probably attributable to the higher etch rates employed in this study (more than twice that of the other researchers), resulting in higher sputter yields.

Sample damage may occur even with moderate etch rates and low incident electron beam energies if the surface of the sample is delicate. This problem was encountered while attempting to study the organic inhibitors on the surface of the alloy, and will be discussed later.

The auger instrument also permits one to do scanning electron microscopy (SEM), elemental mapping, line analysis, and point analysis. SEM provides an image of the surface and with the other techniques permits certain areas or surface features to be examined in detail. Photomicrographs can be taken showing surface features and these can be correlated with auger data.

Material Balance

The majority of corrosion reactions are electrochemical in nature, and thus it is quite natural to utilize electrode methods to study them[26]. A basic disadvantage of this approach is the interference of the electrochemical measurements with the corrosion reactions themselves. The assumption that a freely corroding metal will behave in the same fashion as the metal placed in an electrochemical cell is certainly questionable[27].

Material balance studies do not suffer from this problem since they do not interfere with the corrosion process. This technique, when used in conjunction with the surface analytical techniques, can provide detailed information on the fates of metals involved in the corrosion processes and is helpful in determining mechanisms.

In this study AES is utilized to analyze the corrosion products formed on the metal surface. Atomic absorption spectrophotometry is employed to determine metals lost to solution[28], and microbalance readings are used to monitor weight changes. From these analyses the data for examining the majority of corrosion reactions can be collected. Alloy samples are pretreated

to remove sample history and ensure a clean surface which is representative of the bulk alloy[29]. The samples are weighed prior to corrosion; after corrosion they are dried and reweighed. The corroding medium is analyzed by atomic absorption and the samples are analyzed by AES. The corrosion product is then removed chemically (or mechanically) before measuring the final weight of the alloy sample[30-32]. The data are then combined through mass balance equations to determine the fate of each component during corrosion. The material balance equations are presented in the experimental section.

Due to the low levels of copper and nickel lost to the corroding medium and possible interferences in the seawater, it was necessary to preconcentrate the samples for solution analysis. The method chosen involved passing the seawater over an ion-exchange column which retains heavy metals (Cu, Ni, Cd) while allowing alkali and alkaline earth metals to pass through. The resin chosen was Chelex-100 (Bio-Rad Labs, Richmond, Ca) consisting of a styrene lattice with iminodiacetic acid groups to retain the copper and nickel. If pH is maintained above 5, copper and nickel will be quantitatively removed. After elution with small quantities of nitric acid they are analyzed by atomic absorption[33]. Precipitated metal or insoluble metal complexes will pass through Chelex-100 unretained[34,35], enabling calculation of insoluble as well as soluble corrosion products lost to solution.

Inhibition

The best way to limit corrosion is to select the appropriate metal or alloy for a particular corrosive service. Providing the proper choice has been made there are still methods one can employ or materials one can use to diminish the corrosion, thus prolonging service life and reducing costs.

One method involves changing the corrosive medium. Several changes often employed include (1) lowering temperature, (2) decreasing velocity, (3) removing oxygen or oxidizers, and (4) changing concentration[1]. Care must be taken when applying these methods, as they are not effective in all systems.

Another method useful in many situations is the application of cathodic or anodic protection. Cathodic protection is achieved by supplying electrons to the metal, suppressing metal dissolution and increasing the rate of the cathodic reaction (hydrogen evolution for example). There are two ways to protect a structure cathodically, one is to impress a current and the other is by appropriate galvanic coupling. Such methods are commonly employed to protect buried iron pipes and also hot and cold water tanks[36].

In impressing a current one connects the negative pole of a dc power supply to the structure to be protected. The positive terminal is connected to an inert anode such as graphite. Current passes to the metal structure and corrosion is prevented. Galvanic coupling to a metal anodic to the metal structure to be protected is also effective. In the case of iron or steel, connection is

made to a "sacrificial anode" such as magnesium, which corrodes preferentially and is consumed during protection of the steel.

Anodic protection is relatively new in contrast to cathodic protection and is more complex. It is based on the formation of a protective film on metals by externally applied anodic currents. A requirement for the method to be effective is an active-passive transition. The anodic current shifts the potential from active to passive. A potentiostat is required to maintain the metal at a constant potential with respect to a reference electrode[1]. Advantages of this technique are its applicability in extremely corrosive environments, and its low current requirements.

Paints and other coatings prevent or reduce corrosion and provide the basis for several industries. Coatings can be metallic, inorganic, or organic in nature.

Metallic coatings are generally applied to the object to be protected either by immersion in a molten bath of metal (hot dipping) or by electroplating from an aqueous electrolyte. Coatings may be classified as noble or sacrificial. Noble coatings such as chromium on steel must be carefully prepared with few pores if corrosion of the base metal through galvanic action is to be minimized (Figure 7). To prevent this the coating must be made thick and sometimes the pores filled with an organic lacquer.

Sacrificial coatings such as galvanizing (zinc on iron) protect the base metal cathodically. The degree of porosity is not

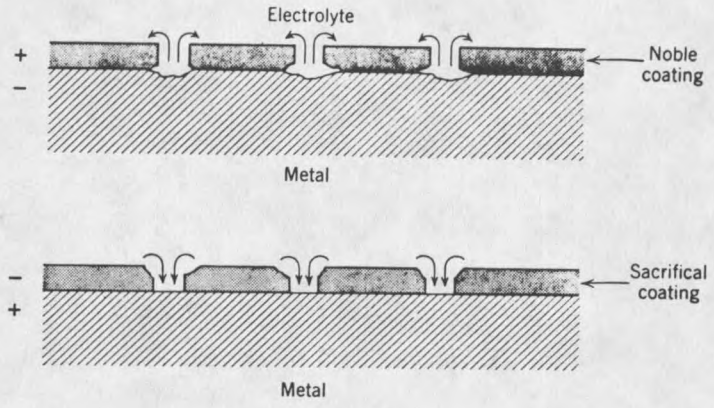


Figure 7. Sketch of Electron Flow at Defects in Noble and Sacrificial Coatings[37].

as critical with sacrificial coatings, but in general the thicker the coating, the longer the cathodic protection will last.

Inorganic coatings include vitreous enamels, portland cement, and chemical conversion coatings. The vitreous enamels are glass coatings fused on metals. They are applied in powdered form to a cleaned metal surface and heated in a furnace to soften the glass and allow it to bond to the metal. They are used mostly on steels, but can also be used on other metals, including copper and its alloys. The glasses are composed of alkali borosilicates and are effective in resisting strong acids and other corrosives.

One criterion in coating technology is agreement of the coefficient of expansions of metal and coating. With heat changes the coating must expand and contract in a fashion similar to that of the metal to avoid cracking and buckling. Cement coatings which are relatively inexpensive, are used widely with steels as the coefficients of expansion are similar. The coatings are applied by

centrifugal casting, troweling, or spraying; and have shown good service records.

Chemical conversion coatings are formed in situ by reactions which involve the metal surface. Examples include phosphate coatings on steel, sulfate coatings resulting from the exposure of lead to sulfuric acid, and oxide coatings on aluminum (anodizing). Such coatings can be very effective in reducing corrosion.

The application of an organic coating which provides a relatively thin barrier between the metal and the environment is the method of choice in many cases. Paints, varnishes, and lacquers protect more metal than any other method, a primary reason being cost effectiveness. The method involves pretreatment of the substrate (cleaning), a primer, the organic coating, and the mode of application, all of which are important for successful preservation[38].

Although coatings represent the largest technique for corrosion prevention, many applications are not amenable to coatings and coating technology. Included are cooling, recirculating, and heating systems; condensation lines; internal combustion engines and turbines; high chloride systems; and systems exposed to acid solutions. Because of environmental factors, extremely corrosive systems, high temperatures, high flow rates, friction, and mechanical wear, it is simply impossible to use coatings to prevent corrosion in many systems.

Some of these systems can be protected with inhibitors, either in solution or in a pretreatment step. An inhibitor is a chemical

that effectively decreases the corrosion rate when added in a small concentration to an environment or pretreated on the surface prior to use. Inhibitors function as chemically or physically adsorbed films which either alter the electrochemical characteristics of the metal or serve as mechanical barriers to corrosion[39]. They may interfere with the anodic or the cathodic reactions, or act as diffusion barriers. In some applications they help prevent fouling and organic layer buildup.

Most corrosion processes can be simply defined by two reactions, as given in equations 7 and 8. The rate of corrosion

$$M \longrightarrow M^{n+} + ne^- \qquad (7)$$

$$ne^- + Ox \longrightarrow Red^- \qquad (8)$$

depends upon the rates of the two conjugate reactions proceeding on the metal surface; the anodic metal dissolution reaction, and the cathodic reaction in assimilation of the electrons liberated by the anodic reaction. Inhibition may be achieved by interference with either or both of these reactions.

There are many different types of inhibitors in use today, depending upon environmental factors and the particular application. Inorganic inhibitors are used primarily in neutral electrolytes, and affect the anodic process and the passive state of the metal. Organic inhibitors on the other hand are used primarily in acid electrolytes. After adsorption, they alter the kinetics of the cathodic reaction[40]. The division on the basis of medium is not complete however, as some inorganic inhibitors are used in acid

systems and some organic inhibitors have applications in neutral electrolytes.

A list of inhibitors as applied to certain metal-environment combinations is given in Table 1. It is important to notice that these inhibitors are specific in terms of the metal, environment, temperature, and the concentration range. Certain inhibitors are considered "safe" while others are "dangerous". If present in too small or too large a concentration some inhibitors will actually stimulate rather than inhibit the corrosion processes. Consequently great care must be taken in inhibitor application.

Anodic inhibitors, compounds that reduce the rate of corrosion by retarding the anodic reaction, are often referred to as passivators. Passivators act as depolarizers and initiate high current densities at anodic areas in excess of $i_{critical}$. Only ions with an oxidizing capacity in the thermodynamic sense (noble oxidation-reduction potential) and which are readily reduced (shallow cathodic polarization curve) may act as passivators, as shown in Figure 8. Only metals which display an active/passive polarization curve are amenable to protection with passivators, and the passivator concentration must be great enough to exceed $i_{critical}$ or stimulation of the corrosion may result. Thus anodic inhibitors or passivators can be "dangerous" and must be applied in the proper concentrations.

# Table 1. Corrosion Inhibitors Reference List[1].

| *Metal* | *Environment* | *Inhibitor* |
|---|---|---|
| Admiralty | Ammonia, 5% | 0.5% hydrofluoric acid |
| Admiralty | Sodium hydroxide, 4° Be | 0.6 moles $H_2S$ per mole NaOH |
| Aluminum | Acid hydrochloric, 1 *N* | 0.003 *M* $\alpha$ phenylacridine, $\beta$ naphthoquinone, acridine, thiourea or 2-phenylquinoline |
| Aluminum | Acid nitric, 2–5% | 0.05% hexamethylene tetramine |
| Aluminum | Acid nitric, 10% | 0.1% hexamethylene tetramine |
| Aluminum | Acid nitric, 10% | 0.1% alkali chromate |
| Aluminum | Acid nitric, 20% | 0.5 hexamethylene tetramine |
| Aluminum | Acid phosphoric | Alkali chromates |
| Aluminum | Acid phosphoric, 20% | 0.5% sodium chromate |
| Aluminum | Acid phosphoric, 20–80% | 1.0% sodium chromate |
| Aluminum | Acid sulphuric, conc. | 5.0% sodium chromate |
| Aluminum | Alcohol anti-freeze | Sodium nitrite and sodium molybdate |
| Aluminum | Bromine water | Sodium silicate |
| Aluminum | Bromoform | Amines |
| Aluminum | Carbon tetrachloride | 0.05% formamide |
| Aluminum | Chlorinated aromatics | 0.1–2.0% nitrochlorobenzene |
| Aluminum | Chlorine water | Sodium silicate |
| Aluminum | Calcium chloride, sat | Alkali silicates |
| Aluminum | Ethanol, hot | Potassium dichromate |
| Aluminum | Ethanol, commercial | 0.03% alkali carbonates, lactates, acetates or borates |
| Aluminum | Ethylene glycol | Sodium tungstate or sodium molybdate |
| Aluminum | Ethylene glycol | Alkali borates and phosphates |
| Aluminum | Ethylene glycol | 0.01–1.0% sodium nitrate |
| Aluminum | Hydrogen peroxide, alkaline | Sodium silicate |
| Aluminum | Hydrogen peroxide | Alkali metal nitrates |
| Aluminum | Hydrogen peroxide | Sodium metasilicate |
| Aluminum | Methyl alcohol | Sodium chlorate plus sodium nitrite |
| Aluminum | Methyl chloride | Water |
| Aluminum | Polyoxyalkene glycol fluids | 2% Emery's dimer acid (dilinoleic acid), 1.25% $N(CHMe_2)_3$, 0.05–0.2% mercaptobenzothiazole |
| Aluminum | Seawater | 0.75% sec. amyl stearate |
| Aluminum | Sodium carbonate, dilute | Sodium fluosilicate |
| Aluminum | Sodium hyroxide, 1% | Alkali silicates |
| Aluminum | Sodium hydroxide, 1% | 3–4% potassium permanganate |
| Aluminum | Sodium hydroxide, 4% | 18% glucose |
| Aluminum | Sodium hypochlorite contained in bleaches | Sodium silicate |
| Aluminum | Sodium acetate | Alkali silicates |
| Aluminum | Sodium chloride, 3.5% | 1% sodium chromate |
| Aluminum | Sodium carbonate, 1% | 0.2% sodium silicate |
| Aluminum | Sodium carbonate, 10% | 0.05% sodium silicate |
| Aluminum | Sodium sulfide | Sulfur |
| Aluminum | Sodium sulfide | 1% sodium metasilicate |
| Aluminum | 50% sodium trichloracetate soln. | 0.5% sodium dichromate |
| Aluminum | Tetrahydrofurfuryl alcohol | 1% sodium nitrate or 0.3% sodium chromate |
| Aluminum | Triethanolamine | 1% sodium metasilicate |
| Brass | Carbon tetrachloride, wet | 0.001–0.1 aniline |
| Brass | Furfural | 0.1% mercaptobenzothiazole |
| Brass | Polyoxyalkene glycol fluids | 2.0% Emery's acid (dilinoleic acid), 1.25% $N(CHMe_2)_3$, 0.05–0.2% mercaptobenzothiazole |
| Brass | 50% sodium trichloracetate soln. | 0.5% sodium dichromate |
| Cadmium plated steel | 55/45 ethylene glycol—water | 1% sodium fluorophosphate |
| Copper | Fatty acids as acetic | $H_2SO_4$, $(COOH)_2$ or $H_2SiF_6$ |
| Copper | Hydrocarbons containing sulfur | P-hydroxybenzophenone |
| Copper | Polyoxyalkene glycol fluids | 2% Emery's acid (dilinoleic acid), 1.25% $N(CHMe_2)_3$, 0.05–0.2% mercaptobenzothiazole |
| Copper & brass | Acid sulfuric, dil | Benzyl thiocyanate |
| Copper & brass | Ethylene glycol | Alkali borates & phosphates |
| Copper & brass | Polyhydric alcohol anti-freeze | 0.4–1.6% $Na_3PO_4$ plus 0.3–0.6 sodium silicate plus 0.2–0.6% sodium mercaptobenzothiazole |
| Copper & brass | Rapeseed soil | Succinic acid |
| Copper & brass | Sulfur in benzene solution | 0.2% 9, 10 anthraquinone |
| Copper & brass | Tetrahydrofurfuryl alcohol | 1% sodium nitrate or 0.3% sodium chromate |
| Copper & brass | Water-alcohol | 0.25% benzoic acid, or 0.25% sodium benzoate at a pH of 7.5–10 |

Table 1 (continued)

| *Metal* | *Environment* | *Inhibitor* |
|---|---|---|
| Galvanized iron | Distilled water | 15 ppm. mixture calcium and zinc metaphosphate |
| Galvanized iron | 55/45 ethylene glycol—water | 0.025% trisodium phosphate |
| Iron | Nitroarylamines | Dibenzylaniline |
| Lead | Carbon tetrachloride, wet | 0.001–0.1% aniline |
| Magnesium | Alcohol | Alkaline metal sulfides |
| Magnesium | Alcohol, methyl | 1% oleic or stearic acid neutralized with ammonia |
| Magnesium | Alcohols, polyhydric | Soluble fluorides at pH 8–10 |
| Magnesium | Glycerine | Alkaline metal sulfides |
| Magnesium | Glycol | Alkaline metal sulfides |
| Magnesium | Trichlorethylene | 0.05% formamide |
| Magnesium | Water | 1% potassium dichromate |
| Monel | Carbon tetrachloride, wet | 0.001–0.1% aniline |
| Monel | Sodium chloride, 0.1% | 0.1% sodium nitrite |
| Monel | Tap water | 0.1% sodium nitrite |
| Nickel & silver | Sodium hypochlorite contained in bleaches | Sodium silicate |
| Stainless steel | Acid sulfuric, 2.5% | 5–20 ppm. $CaSO_4.5H_2O$ |
| Stainless steel | Cyanamide | 50–500 ppm. ammonium phosphate |
| Stainless steel, 18-8 | Potassium permanganate contained in bleaches | Sodium silicate |
| Stainless steel, 18-8 | Sodium chloride, 4% | 0.8% sodium hydroxide |
| Steel | Acid citric | Cadmium salts |
| Steel | Acid sulfuric, dil | Aromatic amines |
| Steel | Acid sulfuric, 60–70% | Arsenic |
| Steel | Acid sulfuric, 80% | 2% boron trifluoride |
| Steel | Aluminum chloride—hydrocarbon complexes formed during isomerization | 0.2–2.0% iodine, hydriodic acid or hydrocarbon iodide |
| Steel | Ammoniacal ammonium nitrate | 0.2% thiourea |
| Steel | Ammonium nitrate—urea solns. | 0.05–0.10% ammonia |
| Steel | Brine containing oxygen | 0.1% ammonium thiocyanate<br>0.001–3.0 methyl, ethyl or propyl substituted dithiocarbamates |
| Steel | Carbon tetrachloride, wet | 0 001–0.1% aniline |
| Steel | Caustic—cresylate solution as in regeneration of refinery caustic wash solutions, 240–260F | 0.1–1.0% trisodium phosphate |
| Steel | Ethyl alcohol, aqueous or pure | 0.03% ethylamine or diethylamine |
| Steel | 55/45 ethylene glycol—water | 0.025% trisodium phosphate |
| Steel | Ethylene glycol | Alkali borates & phosphates |
| Steel | Ethylene glycol | Guanidine or guanidine carbonate |
| Steel | Ethyl alcohol, 70% | 0.15% ammonium carbonate plus 1% ammonium hydroxide |
| Steel | Furfural | 0.1% mercaptobenzothiazole |
| Steel | Halogenated dielectric fluids | 0.05–4% $(\gamma C_4H_9S)_4$ Sn $\gamma(C_4H_9)_2Sn$ or $\gamma C_4H_9S$ $SnPh_3$ |
| Steel | Halogenated organic insulating materials as chlorinated dipheryl | 0.1% 2, 4$(NH_2)_2C_6H_3NHPh$, *o*—$MeH_4NH_2$ or *p*—$NO_2C_6H_4NH_2$ |
| Steel | Herbicides as 2, 4 dinitro—6—alkyl phenols in aromatic oils | 1.0–1.5% furfural |
| Steel | Isopropanol, 30% | 0.03% sodium nitrite plus 0.015% oleic acid |
| Steel | 1:4 methanol—water | To 4 l. water and 1 l. methanol add 1 g. pyridine and 0.05 g. pyragallol |
| Steel | Nitrogen fertilizer solutions | 0.1% ammonium thiocyanate |
| Steel | Phosphoric acid, conc. | 0.01–0.5% dodecylamine or 2 amino bicyclohexyl and 0.001% potassium iodide, potassium iodate or iodacetic acid |
| Steel | Polyoxyalklene glycol fluids | 2% Emery's acid (dilinoleic acid)<br>1.25% $N(CHMe_2)_3$<br>0.05–0.2% mercaptobenzothiazole |
| Steel | Sodium chloride, 0.05% | 0.2% sodium nitrite |
| Steel | 50% sodium trichloracetate soln. | 0.5% sodium dichromate |
| Steel | Sulfide containing brine | Formaldehyde |
| Steel | Tetrahydrofurfuryl alcohol | 1% sodium nitrate or 0.3% sodium chromate |
| Steel | Water | Benzoic acid |
| Steel | Water for flooding operations | Rosin amine |
| Steel | Water saturated hydrocarbons | Sodium nitrite |
| Steel | Water, distilled | Aerosol (an ionic wetting agent) |

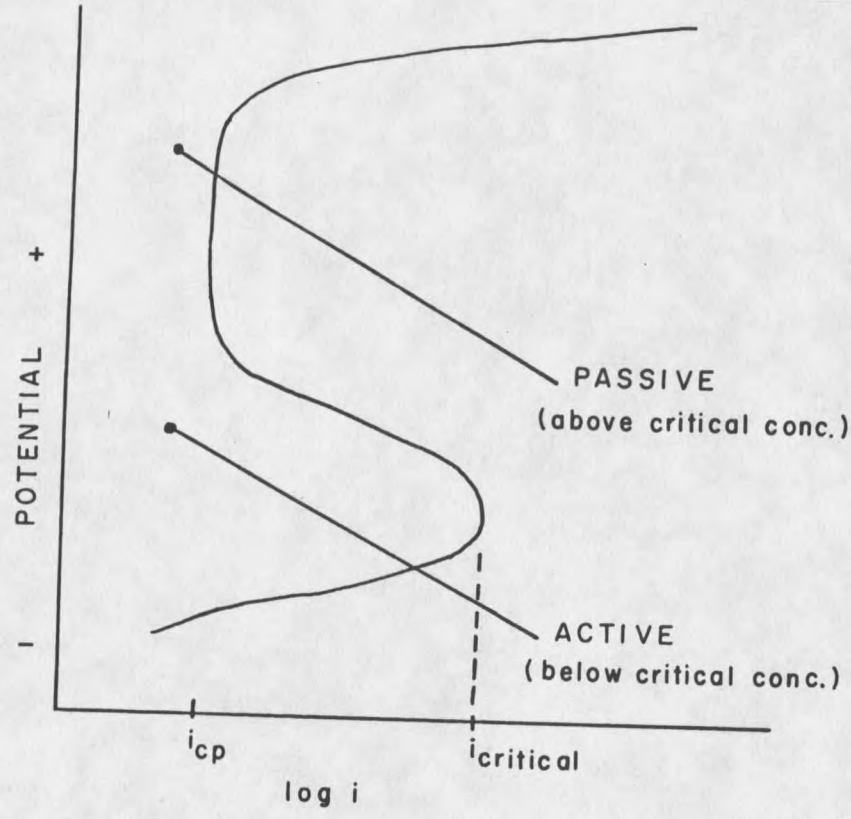


Figure 8. Polarization Curves That Show the Effect of Passivator Concentration on Corrosion.

If ionization of the metal is assumed to be limiting in the anodic dissolution of metals, then the rate of the anodic process can be expressed in terms of the anode current density $i_a$:

$$i_a = k \exp(\alpha n \phi_a F/RT) \qquad (9)$$

where k is the rate constant, $\alpha$ is the transfer coefficient, n is the number of electrons liberated when an ion-atom of metal dissolves, and $\phi_a$ is the anode potential[40]. Thus the more positive the anode potential the greater the dissolution rate will be. An expression for the overvoltage Na of the anodic process is obtained by taking the log of this equation and substituting in the value of

the equilibrium potential:

$$Na = a + b \ln(i_a) \qquad (10)$$

where a and b are constants and $i_a$ is the anode current density.

The rate of the anodic reaction can be described by a Tafel line, until one reaches the passivation potential $\phi_p$ where the Tafel dependence is lost. The reaction rate drops off until one reaches a very low value of the potential of complete passivation $\phi_{cp}$. At this potential the metal becomes completely passive due to a retardation of the anodic process[41].

Examples of anodic inhibitors include sodium benzoate[42], sodium polyphosphate[43], and sodium chromate[44] for passivating steel in neutral solutions. Chromates, phosphates, and borates are employed for passivation of copper and copper alloys in some applications (Table 1) and are also utilized in combination with organic inhibitors.

As mentioned previously, organic inhibitors are used primarily in acid electrolytes and function by adsorption and its effect on the kinetics of the cathodic reaction. They are quite commonly employed during the pickling process of steel. Recently they have found applications in neutral electrolyte solutions, and several are employed for inhibition of copper and copper alloy corrosion. They are also used in lubricating oils, greases, antifreeze for internal combustion engines, and protection of water pipes and heat exchangers.

The majority of organic inhibitors contain nitrogen, sulfur, or oxygen, although several hydrocarbons are employed as well.

The nitrogen-containing compounds include amines, pyridines, the quaternary salts of pyridine bases, and others. The sulfur-containing compounds include mercapto compounds, thiourea, and others. Some inhibitors contain both sulfur and nitrogen. The compounds containing oxygen are generally the aldehydes or alcohols.

Pioneering work in the field of organic inhibitors was performed by Chappell, Roetheli, and McCarthy[45] on quinoline ethiodide protection of iron and steel in sulfuric acid and concluded that inhibition was cathodic. Charles Mann at the University of Minnesota carried out extensive experiments on nitrogen and sulfur containing inhibitors and proposed a comprehensive theory of inhibition by organic compounds[46]. He proposed that these organic inhibitors are all capable of forming onium ions and exist as cations in acid solutions. They are cathodically adsorbed by electrostatic attraction, covering cathodic areas. The resulting film increases resistance to the passage of current by preventing hydrogen ions from reaching the surface. Variations in the inhibiting efficiency of different molecules depends on the extent of adsorption, the cross-sectional area of the molecule, and steric factors. The structure of the ion determines the packing of the ions in the layer which determines the imperviousness to hydrogen ions.

Cathodic polarization studies have supported this theory, but a major problem with these is the high current densities and very negative potentials. These conditions are very different from

the open circuit situation during corrosion, so conclusions regarding these experiments may be in error[47].

There are several problems with acceptance of Mann's theory. One is the change in open circuit potential cathodically upon addition of inhibitors. This may be explained if one assumes the inhibitor effects mainly the anodic reaction, but not the cathodic reaction. Another problem is both anodic and cathodic effects have been found in polarization studies at small current densities[48]. Finally the specific cases where sulfur compounds are more effective inhibitors than corresponding nitrogen compounds is unexplainable with the theory of cathodic inhibition. The foregoing evidence shows other forces besides electrostatic interactions must have some effect.

The difficulties with Mann's theory have led to a theory of general rather than cathodic adsorption, as favored by Hackerman and Mackrides[49]. Adsorption is postulated to be both physical and chemical in nature. Physical adsorption is a direct result of weak van der Wals forces over the entire metal surface. These dispersion forces, together with chemisorption at cathodic areas, contribute to the overall inhibition. The chemisorption is a result of sharing a pair of electrons from the inhibitor with the metal. The chemisorptive bonds may cause inhibition either by decreasing the metal dissolution or by increasing the activation overpotential for hydrogen discharge.

Although there is no particular reason why the effect of chemisorbed inhibitors should be greater on anodes than on

cathodes, experiment indicates the action is largely anodic (cathodic shift of open circuit potential on addition of inhibitors). The anodic polarization is basically chemisorption with stabilization of the metal ion in the surface lattice, or surface complexation. Overall the inhibition can be considered to be a result of (a) increased resistance to current flow (electrostatic adsorption at cathodic areas) and (b) anodic polarization (chemisorption). Which effect contributes more depends upon the particular inhibitor/metal combination.

Three groups of organic inhibitors may be identified at this point. The first group consists of compounds which function by polarizing anodic dissolution, such as the sulfides. Members of the second group are mixed inhibitors, functioning both by general adsorption (cathodic polarization) and by chemisorptive stabilization of the metal ions in the lattice. The amines and thiols are typical of this group. Cathodic polarizers make up the third group. They cannot function by chemisorption as there is no possibility for electron transfer. Quaternary amine salts are an example.

Chemisorptive bond formation is intimately related to the nature of the metal as well as the adsorbing inhibitor. The strength of the bonding depends on the electronic structure of the functional group of the inhibitor as well as the metal. This bonding may be described as surface complex formation. Unfilled atomic orbitals on the metal are a prerequisite, as is the availability of electrons from the adsorbed group for bond

formation. This is a function of the electron density and polarizability of the adsorbed functional group or atom in the molecule which is bonded to the metal.

It should be noted at this point that chemisorption, like other chemical reactions, is reversible. Thus the extent of chemisorption is a function of the solubility of the inhibitor; the less soluble the inhibitor in the corrosive medium, the greater the extent of chemisorption.

## Purpose of Investigation

Cupro-nickel alloys are used extensively in marine applications because of their excellent corrosion resistance and for this reason were chosen for study. The alloy derives its corrosion resistance from the thin cuprous oxide layer which forms upon exposure to seawater. This corrosion resistance may be greatly improved with the addition of organic inhibitors, and consequently this inhibition is of great practical significance.

Four organic compounds were chosen for study: mercaptothiazoline (MT), mercaptobenzothiazole (MBT), mercaptobenzimidazole (MBI), and mercaptobenzoxazole (MBO). The first two (MT and MBT) were selected to evaluate the effects of an additional aromatic ring on inhibition. The three larger molecules (MBT, MBI, and MBO) were chosen to investigate the effect of variation of the heteroatom $\beta$ to the mercapto sulfur on the ability of these compounds to inhibit cupro-nickel alloy corrosion.

In order to evaluate these inhibitors it was necessary to characterize the corrosion behavior of the 90/10 cupro-nickel alloy without the inhibitors present. Several parameters of particular interest were identified, including exposure, temperature, salinity, and dissolved oxygen.

Because of possible interferences of electrochemical measurements with the corrosion processes, alternate methods to study the corrosion were devised. A material balance technique was developed in conjunction with surface analytical measurements to fully characterize the fates of metals in the corrosion. This required the use of a microbalance, ion exchange preconcentration coupled with atomic absorption spectrophotometry, and scanning auger microprobe analysis.

# EXPERIMENTAL

## Coupon Preparation

Specimens of 90/10 cupro-nickel alloy (CDA-706) were cut from 13 mm I.D., 16 mm O.D. tubular stock with a fine toothed metal saw. The wall sections were cut and filed to a 8 mm width and 145° arc, then fitted to a 15 mm glass test tube by removing sharp edges and burrs. The resulting coupon dimensions are shown in Figure 9. Once cut the coupons were pretreated and then placed in a corrosion cell.

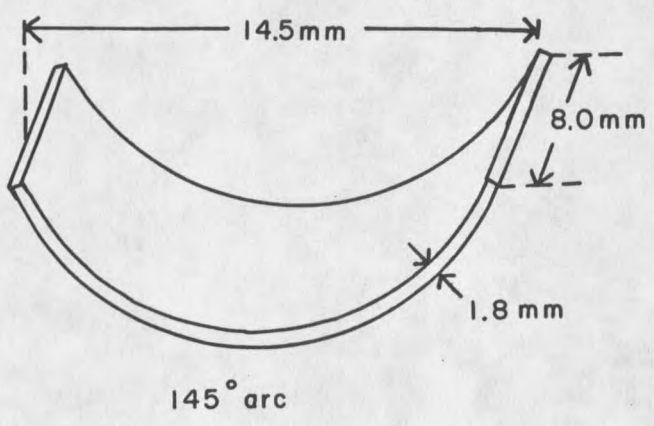


Figure 9. Coupon Dimensions.

## Reactor Design

Two types of corrosion reactors were employed in this study. The simplest was the stirred beaker shown in Figure 10. This reactor was used primarily for experimentation utilizing mass balance and the analysis of solution losses, where it was

experimentally unfeasible to use large volumes of seawater.

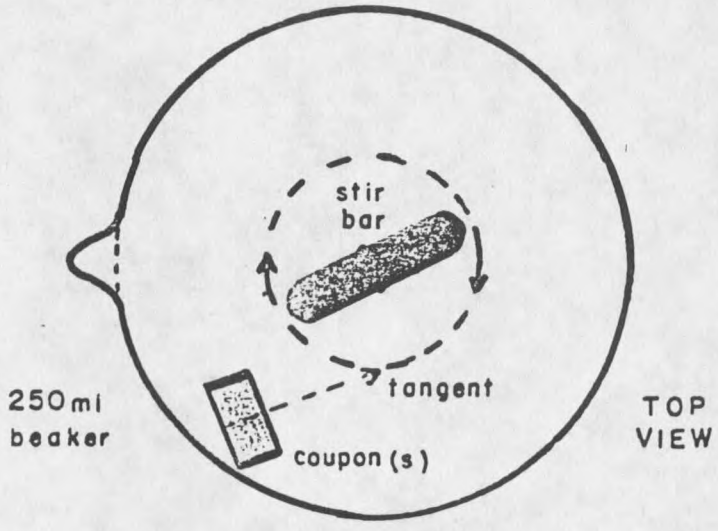


Figure 10. Stirred Beaker Corrosion Reactor.

The stirred beaker corrosion reactor consists of a 250 ml beaker and a one inch teflon coated stirbar. The volume of seawater was maintained at 150 ml and the stir rate was controlled by a stirring plate to maintain a constant flow past the coupon. The coupon was placed along the outer edge of the beaker with its trough in line with the direction of flow of seawater in the beaker. Temperature was maintained by the use of a small water bath into which the stirred beaker was placed.

Although the stirred beaker reactor has the advantage of simplicity and utilizes only a small volume of seawater, it has significant disadvantages including the inability to control atmosphere and dissolved gases and the inability to monitor and control flow rates. For these reasons irreproducibility and

patchiness of corrosion product layers on coupons, especially during longer exposure times, can result. Consequently the recirculating tubular flow corrosion reactor shown in Figure 11 was designed by Dobb[50]. The major components were a pumping system, holding reservoir, and corrosion cell. From the reservoir the seawater was pumped through the corrosion cell and back into the reservoir via 5 mm I.D. tygon tubing. The holding reservoir was a 2L Erlenmeyer flask, and the corrosion cell a 15 mm I.D. x 15 cm test tube with a 6 mm I.D. x 10 cm glass tube linearly joined to the rounded end of the test tube. The arrangement formed a small tube to large tube expansion. Coupons were placed 5 cm from the open end of the large tube, which was then placed inside a 500 ml Erlenmeyer filter flask to prevent gravity effects on flow patterns past the coupon.

A 1/15 horsepower Fisher Scientifc Model MD1-30T recirculating pump was utilized to promote flow of seawater past the coupons. The pump is magnetically driven with a seal-less polypropylene impeller housed in a polypropylene casing, the maximum capacity is 24 liters per minute at 3000 rpm. Flow was regulated by means of restrictors as shown. These were sections of soft glass tubing drawn in a flame to form constrictions of various sizes and calibrated with a graduated cylinder and stopwatch.

The holding reservoir was temperature controlled by means of a water bath, the dissolved oxygen content during longer testing (>12 hours) was maintained by means of a gas bubbler consisting of a 40 mm diameter sintered glass disk and tube. A 5 hole #10 stopper at the top of the holding reservoir allowed for entering and leaving

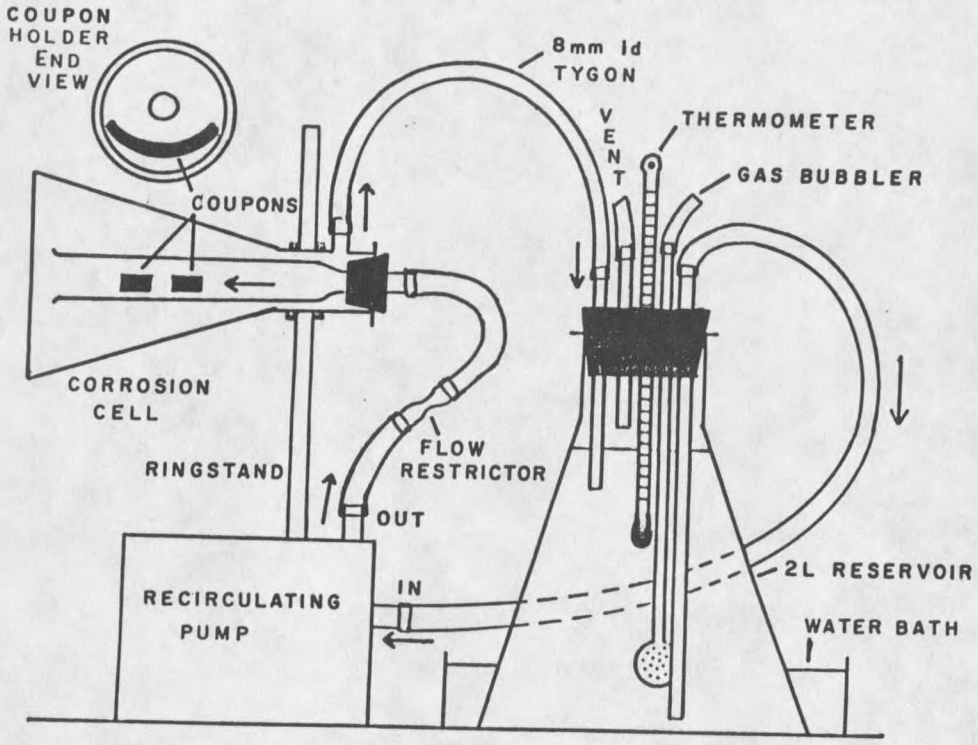


Figure 11. Tubular Flow Corrosion Reactor.

flow tubes, a thermometer, the gas bubbler, and a vent tube which could be open or closed. The reservoir was large enough to approximate once-through flow conditions. This was necessary so the seawater would not be affected substantially by the corroding coupons and the seawater chemistry altered.

Pretreatment of Coupons

Pretreatment of the samples was found to be necessary to minimize the effect of different sample histories and to ensure tarnishing behavior is dependent only on alloy composition. The effects of roughness, degreasing, acid pickling, and sample storage were investigated and are reported in a later section. The recommended pretreatment procedure is as follows:

1. Abrade the surface of the coupon with the 600 grit SiC emery paper to remove previous scratches and ensure homogeneous sample roughness between coupons.
2. Degrease the sample in reagent grade acetone by swirling in a small beaker for one minute. Rinse with fresh acetone and let dry.
3. Pickle the sample in 25% $HNO_3$ for five seconds, and rinse immediately afterwards with doubly distilled water.
4. Either place the sample directly into the corrosion cell or dry with tissue and store.
5. Store the coupons in dessicated vials under nitrogen.

Teflon coated tweezers were employed for sample handling to avoid contamination. After corrosion each sample was rinsed in doubly distilled water, dried with tissue, and stored in a dessicated vial under nitrogen prior to analysis by scanning auger microprobe.

Parameter Measurement and Variation

For the material balance studies several parameters were determined to be of importance. These included variation of exposure time, temperature, salinity, and dissolved oxygen. For comparison purposes between the 90/10 CuNi alloy and work done on the 70/30 CuNi alloy[50], a set of base conditions were decided upon. While one particular parameter was varied all others were kept constant so as to ensure that corrosion effects could be properly assessed. Without a set of base conditions the number of combinations of parameter variations would have been prohibitively large.

The reference set of conditions were 1/3 strength salinity, saturated dissolved oxygen, pH = 8.0, T = 30°C, flow = 15 cm/sec, and 30 minutes exposure time.

The seawaters used in this study included several samples of Pacific Ocean water from Puget Sound, WA, Westport, WA, and artificial ocean water[51]. Salinity was varied by dilution with doubly distilled water and was determined by Mohr titration with standard $AgNO_3$ solution[52].

Temperature was varied by means of a water bath, hot plate, and ice for cooling below room temperature. Each temperature was held constant within ± 1°C.

Time was monitored with a stopwatch. A single flow rate of 15 cm/sec was utilized. This flow rate was characterized in previous work[50] on corrosion of 70/30 cupro-nickel alloy in seawater.

Solution pH was monitored with an Orion combination pH electrode (model 91-05) and a Corning model 130 pH meter. Varian buffer solutions were utilized for standardization and solution pH was modified by addition of standard HCl or NaOH.

Dissolved oxygen was varied by nitrogen purging of the solutions and monitored with a Yellow Springs dissolved oxygen probe.

Auger Analysis

The scanning auger microprobe was a Physical Electronics PHI model 595 (Eden Prairie, MN) at the Center for Research in Surface Science and Submicron Analysis (CRISS) facility at Montana State

University. It consists of a sample introduction system, an ultra high vacuum housing, a cylindrical-mirror electron energy analyzer (single pass) with an integral, coaxially mounted electron gun (1.5 to 30 KV), a 10 KV ion gun for sputter etching, a TV monitor and storage scope for secondary electron imaging and micrographs, and a fully computerized data aquisition system (DEC-PDP 11/04).

Sample manipulation and alignment is achieved by manual control in the X, Y and Z directions of the sample carousel. The carousel is capable of holding 12 samples on 60° sample holders. Special stainless steel clips for securing the samples to the holders were designed by Dobb[50]. The system is microprocessor controlled for focussing electron optics. Data collection and storage involved two dual density floppy disks, and hard copies of the graphics display terminal were obtained by means of a dry silver copier.

The basic analysis procedure begins with securing samples in the sample holders and loading them on the sample carousel. After the samples are loaded, the pressure is reduced to $10^{-9}$ - $10^{-10}$ torr by diffusion and ion pumps. The sample is brought to the focal point of the electron gun and cylindrical mirror analyzer by energy analyzing backscattered electrons at 3 KV beam voltage, a technique called elastic peak adjustment.

The ion gun is focussed and aligned with the electron beam by measuring the ion current in a device called a faraday cup, a ceramically insulated molybdenum cup for collection of ions. This

procedure was necessary to ensure that data collection during depth profiling was taken from the center of the sputter crater.

General surveys were taken of the sample's surface with the analysis conditions given in Table 2. If interesting features were noticed scanning electron micrographs of the surface were taken at various magnifications.

Table 2. Auger Analysis Conditions.

| Parameter | Value |
|---|---|
| Beam Voltage | 5.00 KV |
| Filament Current | 1.65 A |
| Beam Current | 0.35 μA |
| Emission Current | 75 μA (optimized) |
| Emission Current | 190 V (optimized) |
| Magnification | 1000 X |
| Beam Current Density | 6.5 $\mu A/cm^2$ |
| Aperture | Large |
| Vacuum | $10^{-9}$ - $10^{-10}$ torr |

After the surfaces were surveyed for qualitative information, the samples were depth profiled with the ion gun to gain quantitative information about the corrosion products as a function of depth. To calibrate the ion sputtering time with depth in angstroms, standards of 1000 Å $SiO_2$ on Si and 1500 Å $Ta_2O_5$ on Ta

were employed. A typical depth profile of $SiO_2$ on Si is shown in Figure 12. The 1000 Å of $SiO_2$ are completely sputtered away in approximately 16 minutes, as the intensity of oxygen drops off to zero. This corresponds to an etch rate of roughly 60 Å/min and is achieved by the ion beam conditions given in Table 3. The assumption that $Cu_2O$ and $SiO_2$ are sputtered away at approximately the same rate under these conditions is made at this juncture. This was necessary as standards of $Cu_2O$ were not available. This etch rate was found to be quite effective for the samples in this study, although profiling times approached 1 hour for samples corroded 2 to 4 days. The depth profile was taken until the oxide peak disappeared and only base metals were detected.

Table 3. Argon Ion Beam Conditions.

| Parameter | Value |
|---|---|
| Ion Voltage | 1.5 KV |
| Condensor Lens | 820 (optimized) |
| Objective Lens | 900 (optimized) |
| Raster Size | 1.8 mm x 1.8 mm |
| Ion Current Density | 300 $\mu A/cm^2$ |
| Etch Rate ($SiO_2$) | ~60 Å/min |
| Argon Pressure | 20 mPa |

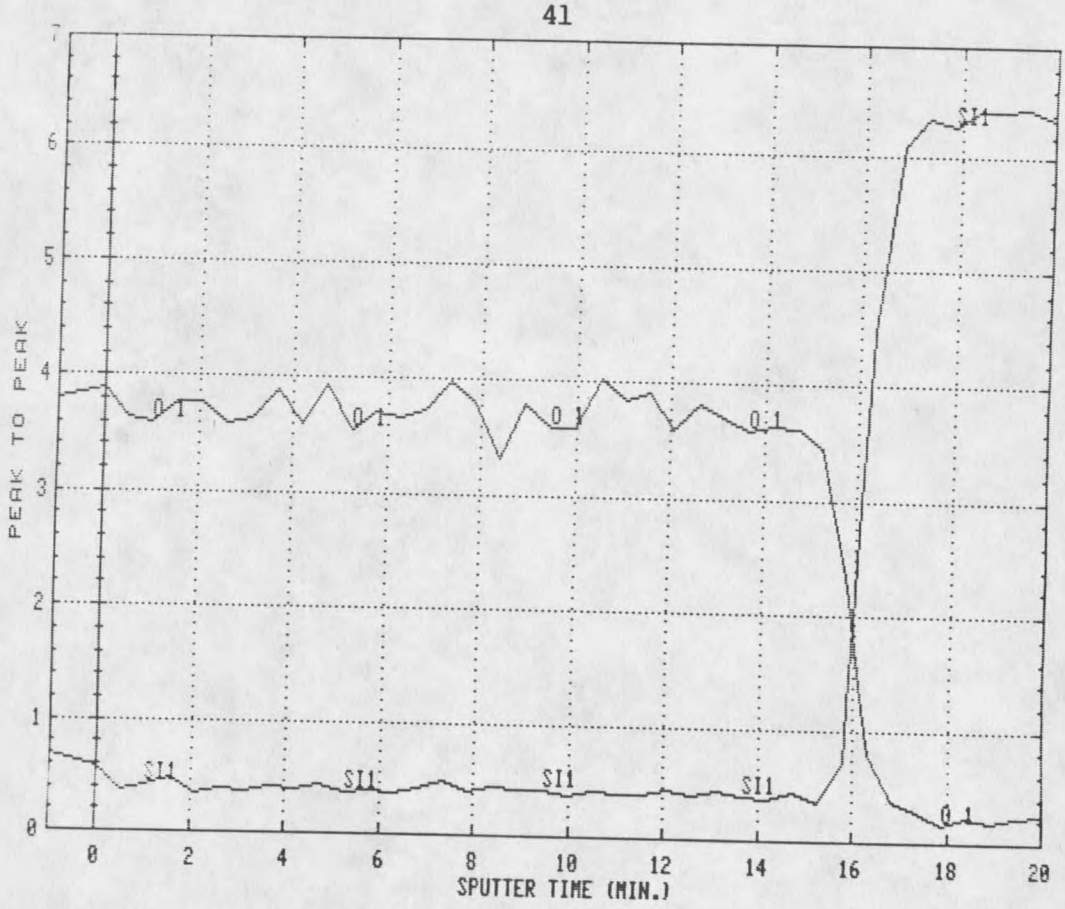


Figure 12. Depth Profile of 1000 Å $SiO_2$ on Si.

Taking data in depth profile mode required setting voltage "windows" for the data aquisition system to measure the peak to peak heights in the differential spectra. The multiplex data parameters for O, Ni, Cu, and Si (in calibration) are given in Table 4. Other elements detected occasionally were C, Cl, and S; but since they usually were sputtered away during the first minute they were not utilized routinely. Depth profiles overcrowded with elemental curves are very difficult to interpret.

The auger data collected during the course of this study is stored both on floppy disks and in hardcopy form in several laboratory notebooks. The volume of data collected to too large to

Table 4. Multiplex Data Parameters.

| Element | O1 | Ni2 | Cu1 | Si1 |
|---|---|---|---|---|
| Lower Limit (eV) | 493 | 755 | 898 | 70 |
| Range (eV) | 30 | 30 | 35 | 30 |
| Volts/Step | 1.00 | 1.00 | 1.00 | 1.00 |
| Time/Step (ms) | 100 | 100 | 100 | 100 |
| Sweeps | 1 | 1 | 1 | 1 |

include in detail in this thesis, so referral to these sources is made here. A hand calculator program for conversion of raw auger peak to peak data into atomic concentration percent was written by Dobb[50] and utilized for all depth profiles collected. This was necessary as the auger computer had no provisions to correct for the of Cu contribution to the Ni peak. Although the principal peak for Ni is at 848 eV (Figure 13), the Cu peak in this region (Figure 14) is too great an interference. We proceeded by utilizing the Ni peak at 783 eV and correcting for the Cu overlap (776 eV) by equation 11.

$$\text{Ni p-p (corrected)} = \text{Ni p-p (uncorrected)} - (.17)\,\text{Cu p-p} \quad (11)$$

The factor of .17 was calculated by a linear method employing standards. The multiplexing window for oxygen (Table 4) included the main peak at 503 eV as shown in Figure 15.

Additional information on scanning auger microscopy can be found in the Auger Handbook[16] and other surface analysis reference material[53,54].

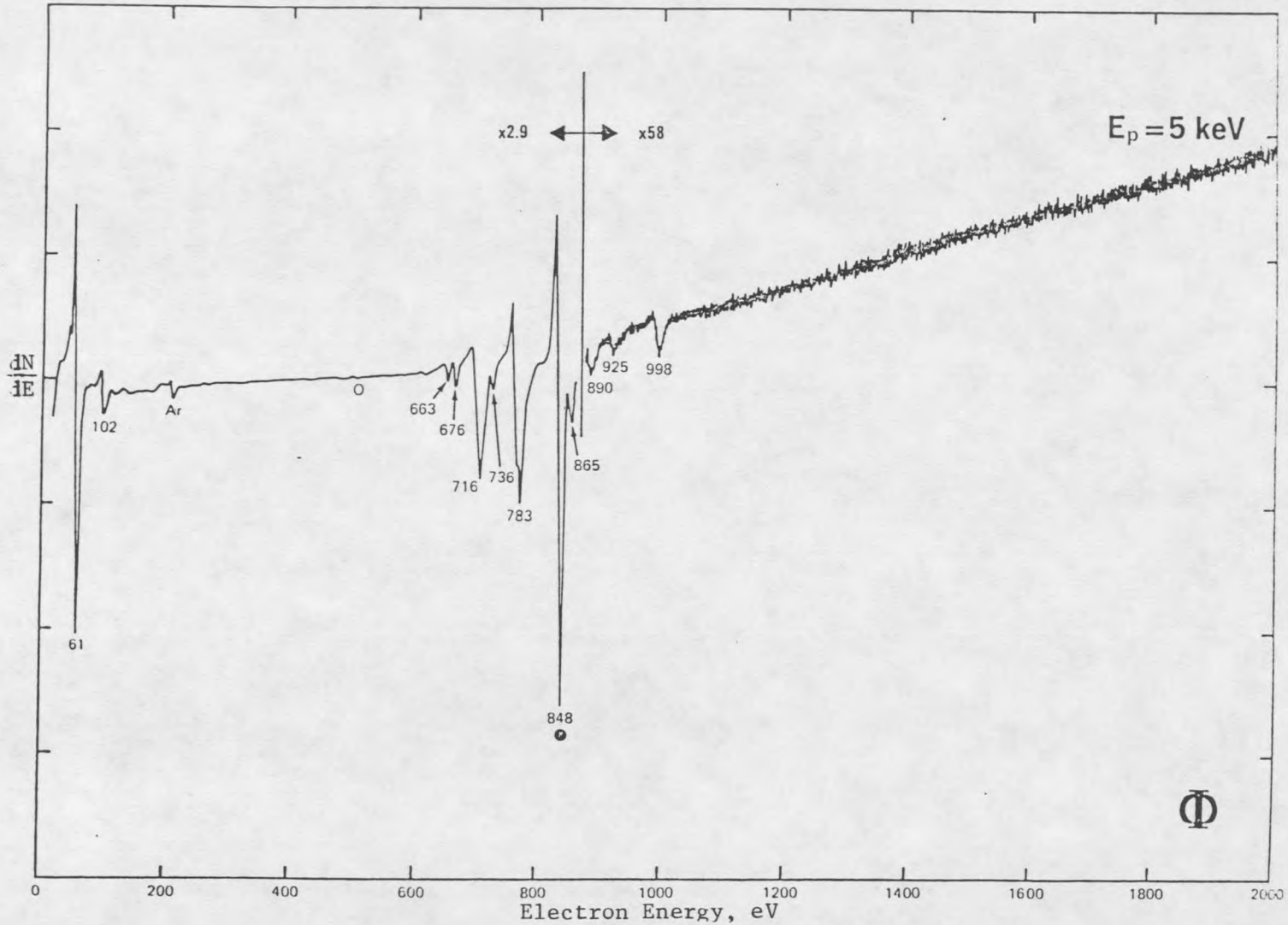


Figure 13. Standard Auger Spectra for Nickel[16].

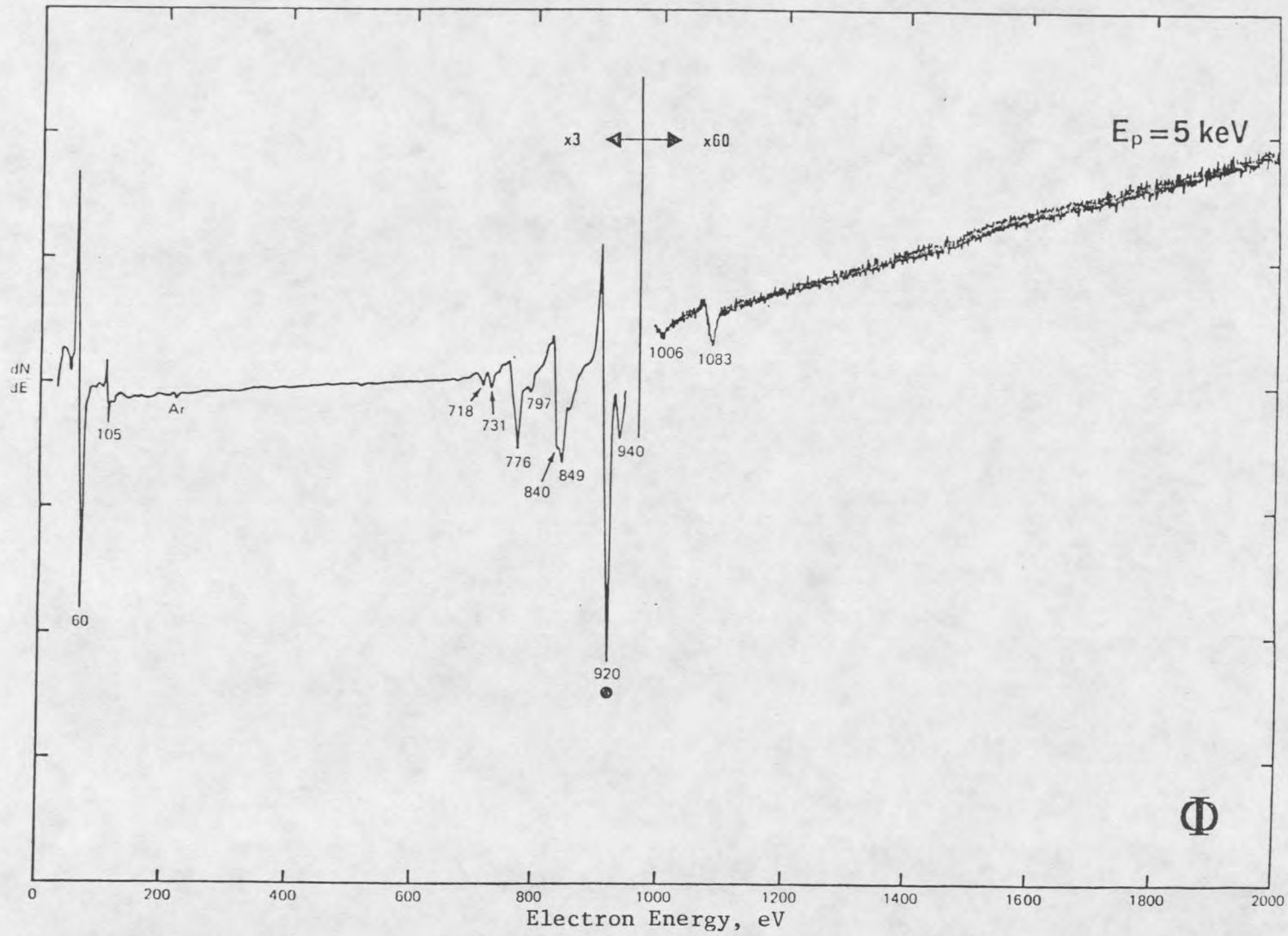


Figure 14. Standard Auger Spectra for Copper[16].

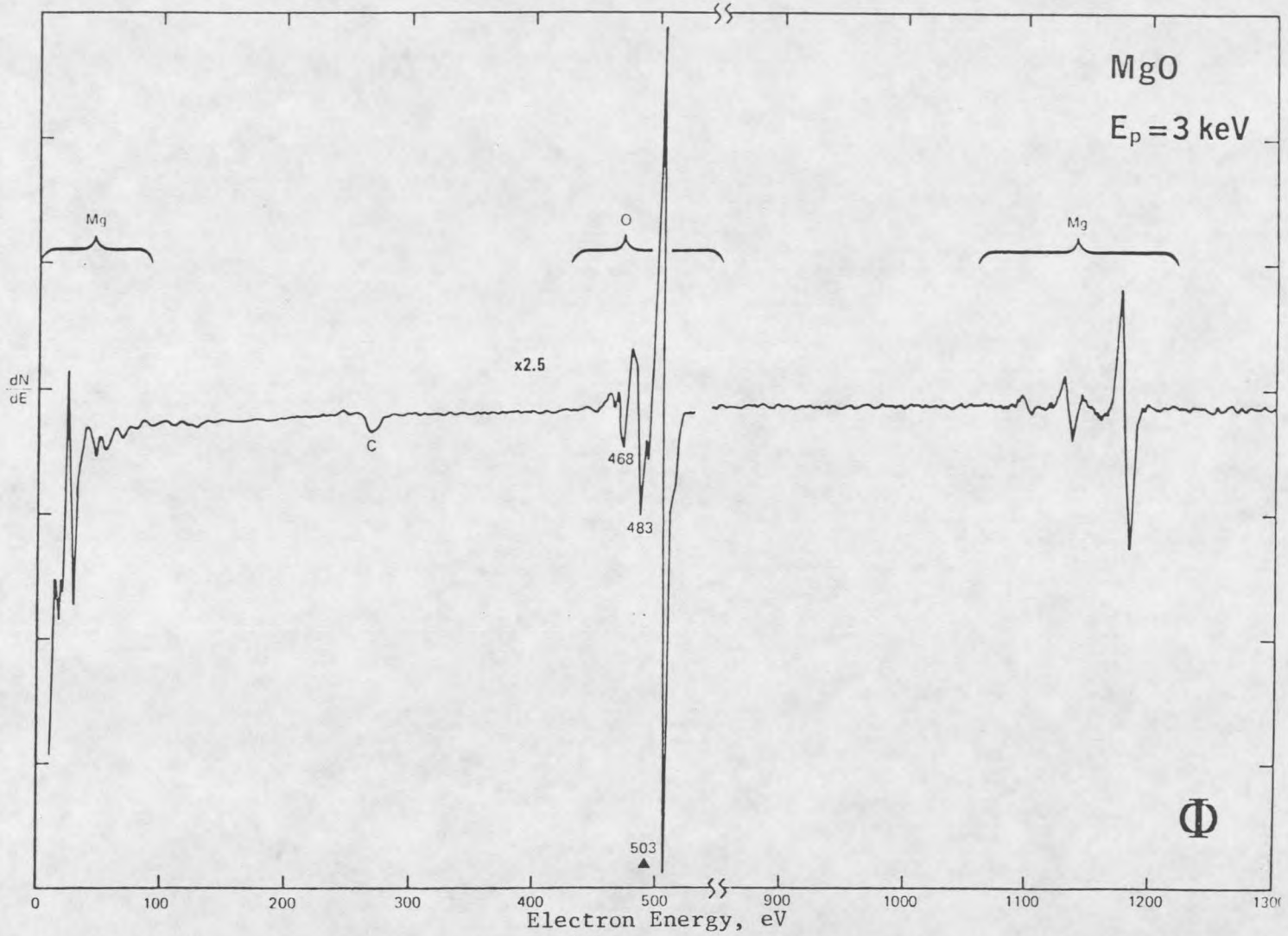


Figure 15. Standard Auger Spectra for Oxygen[16].

Material Balance Derivations

The analysis procedure for material balance is shown in Figure 16. Samples were weighed dry after pretreatment, corrosion, auger analysis, and corrosion product removal (5 second dip in 1:1 HCl). Weighings were taken in triplicate on a Mettler microbalance (Mettler Instrument Corp., Heightstown, NJ) and averaged, allowing precision of $\pm$ 1 $\mu$g for samples up to 20 g.

Because of low metal ion levels the seawater solutions were not analyzed directly. Instead, copper and nickel ions were removed by chelation with Chelex-100 (Bio Rad Labs, Richmond, Ca), utilizing the resin column shown in Figure 17. Volumes of seawater were passed over the 10 cm x 2 $cm^2$ volume, and rinsed with doubly distilled water. The metals were eluted with 20 mls of 2 N $HNO_3$ and analyzed by atomic absorption on a Varian Techtron model 1100 AA spectrophotometer. The atomic absorption conditions are given in Table 5.

To describe the fate of the metals involved in the corrosion processes using a material balance technique in conjunction with AES, it is necessary to introduce several terms. Those listed in Table 6 include weights directly from microbalance measurements, weights derived from atomic absorption solution analysis, empirical values specific to the alloy studied, auger analysis parameters, and weights derived from experimental data following calculations. Although many terms are introduced, these are the minimum required to describe the weight and composition of the corrosion product as

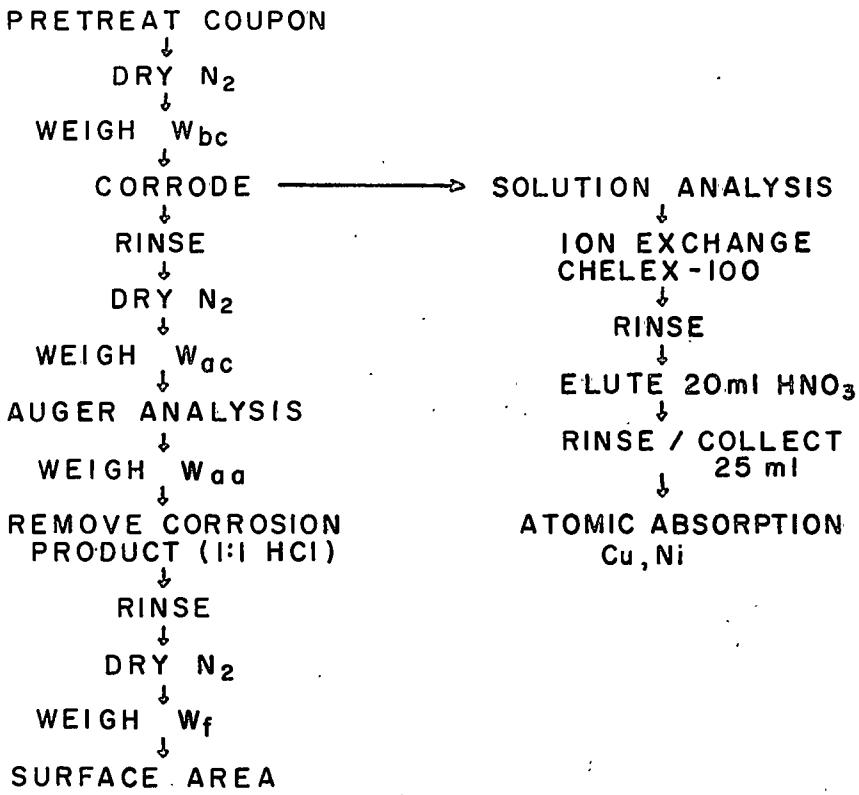


Figure 16. Material Balance Flowchart.

Table 5. Atomic Absorption Conditions for Cu and Ni.

| Parameter | Cu | Ni |
|---|---|---|
| Wavelength (nm) | 324.7 | 232.0 |
| Slit Width (nm) | 0.2 | 0.2 |
| Sensitivity (mg/l) | 0.04 | 0.066 |
| Detection Limit (mg/l) | 0.003 | 0.008 |
| Lamp Current (ma) | 3 | 5 |
| Flame - Air/Acetylene Oxidizing | | |

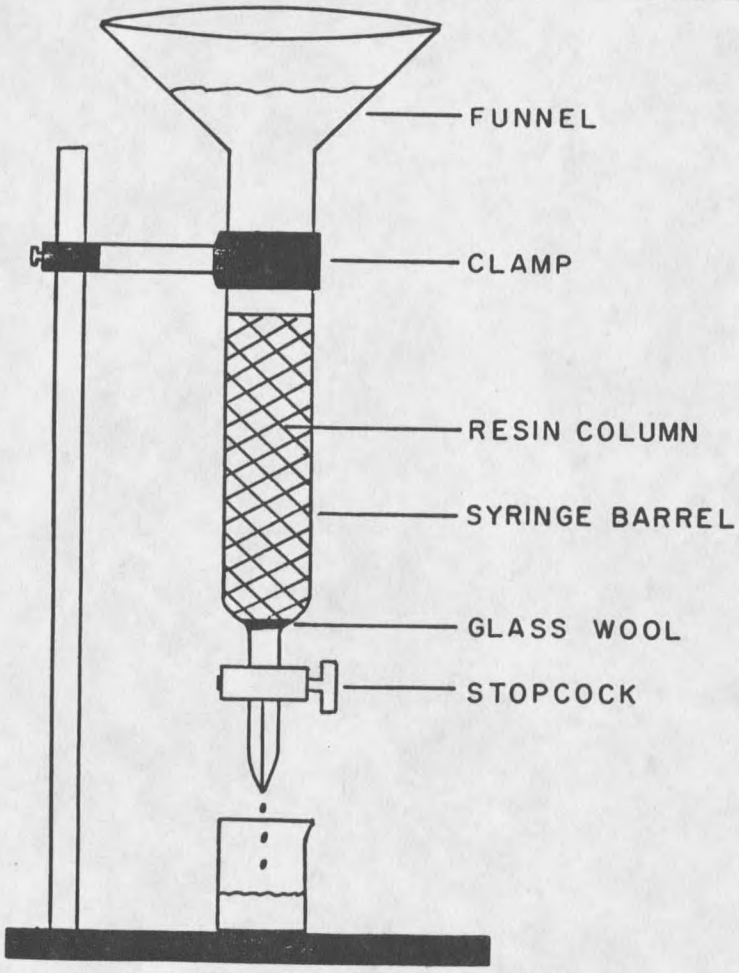


Figure 17. Resin Column for Recovery of Copper and Nickel.

well as the quantity of soluble and insoluble metals lost to solution.

The series of derivations which follow are specific for copper-nickel alloys corroding in seawater. These equations may be adapted to alternate systems, providing one has the capability to analyze for the particular metals lost to solution.

The corrosion product weight (Wcp) is the difference between the weight after corrosion (Wac) and the final weight after

Table 6. Definition of Material Balance Terms.

| | |
|---|---|
| $W_{bc}$ | Weight before corrosion |
| Wac | Weight after corrosion |
| Waa | Weight after auger analysis |
| Wf | Weight after corrosion product removal |
| Wcp | Weight of corrosion product on coupon |
| Wcu | Weight of copper in corrosion product |
| Wni | Weight of nickel in corrosion product |
| Wo | Weight of oxygen in corrosion product |
| Ws | Weight loss of alloy to solution |
| Wsc | Weight of soluble copper in solution |
| Wsn | Weight of soluble nickel in solution |
| Wic | Weight of insoluble copper lost to solution |
| Win | Weight of insoluble nickel lost to solution |
| Wlr | Alloy weight loss during corrosion product removal |
| Wla | Alloy weight loss during auger analysis |
| Fcu | Fraction of copper in alloy |
| Fni | Fraction of nickel in alloy |
| A | Geometrical surface area of coupon |
| As | Area of sputter etch crater |
| Aa | Auger analysis area |
| Oa | Oxygen area under profile (corrected) |
| Of | Oxygen area to weight factor |
| Capc | Copper atomic percent concentration |
| Napc | Nickel atomic percent concentration |
| Oapc | Oxygen atomic percent concentration |

corrosion product removal (Wf), less any metal losses between weighings.

$$Wcp = Wac - Wf - Wla - Wlr \qquad (12)$$

Wlr is the metal loss which occurs while removing the corrosion product with 1:1 HCl. It was experimentally determined by dipping a clean, uncorroded coupon into 1:1 HCl for 5 seconds, and was found to be 1.0 µg ± 0.8 µg.

Wla is the metal loss during auger analysis and results from scratches during loading of coupons into sample holder clips, and

from sputter etching into base metal during depth profiling. The scratches which occur while fitting the samples into the clips are very low in surface area, and hence the corrosion product lost can be ignored. Corrosion product lost while sputter etching is calculated from the ratio of sputtering area (As) to the total surface area (A), multiplied by the weight of corrosion product (Wcp). The metal loss (Wla) is then calculated as the difference between the weight after corrosion (Wac) and the weight after auger analysis (Waa), and subtracting corrosion product lost while sputtering.

$$Wla = Wac - Waa - \frac{As}{A} Wcp \qquad (13)$$

The area of the sputter crater was determined to be 0.054 $cm^2$, and the average surface area of the coupons by caliper measurement was 3.37 $cm^2$. This gives the ratio $As/A \tilde{=} 0.016$, and substitution of calculated values into (12) and (13) and combining gives:

$$Wcp = Wac - Wf - (Wac - Waa - 0.016\ Wcp) - 1.0\ ug \qquad (14)$$

which upon rearrangement yields:

$$Wcp = \frac{Waa - Wf - Wlr}{1 - \frac{As}{A}} = \frac{Waa - Wf - 1.0}{0.984} \qquad (15)$$

Note that all gram weights must be converted to micrograms for these calculations.

The surveys taken on corroded coupons reveal the corrosion products are principally composed of copper, nickel, and oxygen.

Hence we may describe Wcp as the sum of the weights of elements composing the layer.

$$Wcp = Wcu + Wni + Wo \qquad (16)$$

There are two methods to determine the weight of oxygen in the corrosion product (Wo). The first involves determining the area under the oxide depth profile ($O_a$) as shown in Figure 18. This area in At%·Å units is proportional to the weight of oxide in the auger analysis area, and thus when multiplied by the ratio of coupon surface area (A=3.37 $cm^2$) to analysis area (Aa = 4.37 x $10^{-4}$ $cm^2$ at 1000x magnification) is proportional to Wo.

$$Wo = Of \times Oa \frac{A}{Aa} \qquad (17)$$

The oxygen area (Oa) is calculated by conversion of the sputter time axis to Å by the etch rate in Å/min. The resulting area units are converted to weights by the oxygen area to weight factor, Of. This constant has been calculated from the lattice parameters of $Cu_2O$ and NiO, which comprise the oxide layer[55]. The unit conversion factors were determined[50] to be 0.895 x $10^{-13}$ g/AT%Å for $Cu_2O$ and 1.275 x $10^{-13}$ g/AT% Å for NiO. If we assume the corrosion product to be primarily $Cu_2O$ in a ratio of 3:1 $Cu_2O$:NiO, then:

$$Of = \frac{3(0.895 \times 10^{-13}\ g/AT\%Å) + (1.275 \times 10^{-13}\ g(AT\%\ Å)}{4} \qquad (18)$$

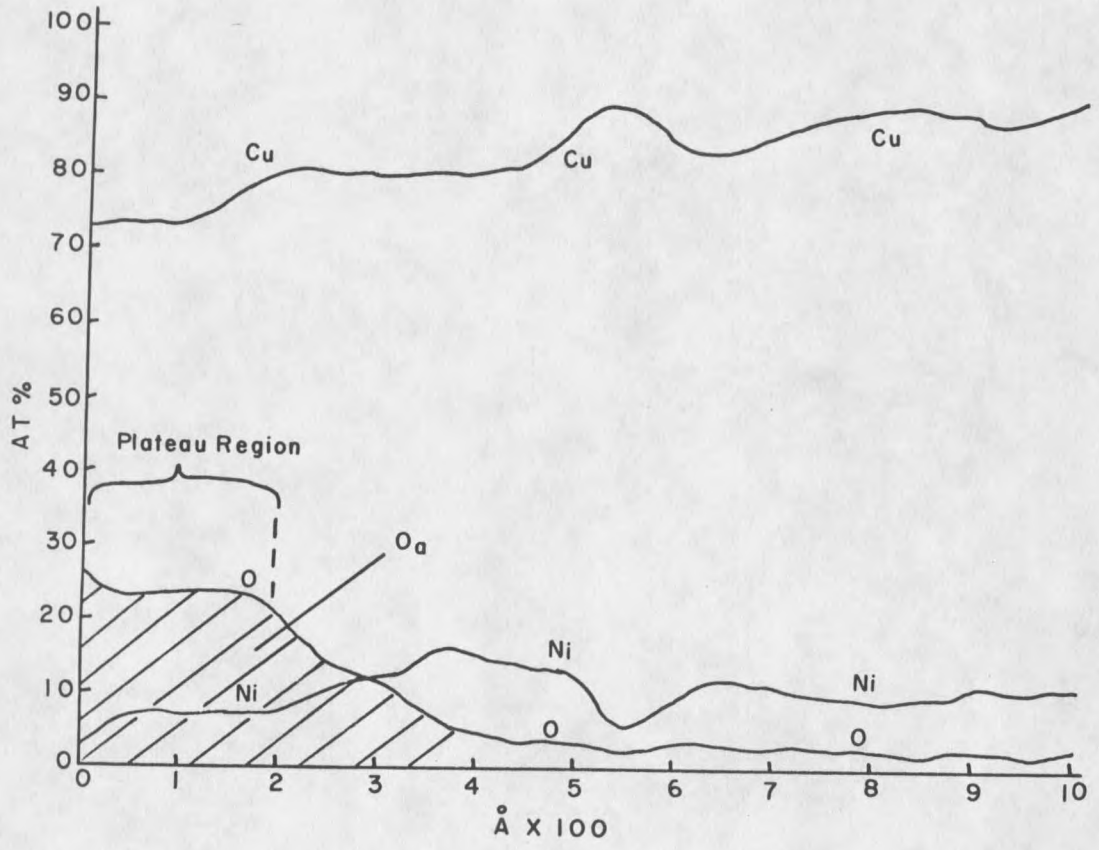


Figure 18. Auger Depth Profile of Coupon Corroded Under Base Conditions.

By conversion of units to μg we get:

$$Of = 9.9 \times 10^{-8} \text{ μg O/AT\%·Å} \qquad (19)$$

It should be mentioned that $Cu_2O$ formed on cupro-nickel alloys can accept varying quantities of $Ni^{2+}$ without significant changes in crystal structure[56]. This suggests that accurate weighting factors are unnecessary.

Substitution of the calculated values for A, Aa, and Of into (17) gives:

$$Wo = Oa \times 7.63 \times 10^{-4} \text{ ug O/AT\%} \cdot \text{Å} \qquad (20)$$

The second method for determination of the weight of oxygen in the corrosion product film is by an empirical rather than a theoretical means. The weight of corrosion product has been plotted versus the weight of oxygen in the corrosion product as shown in Figure 19. The relationship was linear with a slope of 14.21 and a correlation coefficient of .975. Thus when the weight of corrosion product has been determined we may evaluate Wo by the theoretical method or by substitution into equation (21).

$$Wcp = 14.21 \times Wo \qquad (21)$$

The two methods can be employed as checks for accuracy, and it is interesting to note that with equations (20) and (21) one can estimate the weight of corrosion product without weighing by utilization of auger data alone.

In the area of the plateau region (Figure 18) we may calculate the relative atomic concentration percent of each element, Capc, Napc, and Oapc for copper, nickel, and oxygen respectively. The calculations involve the relative sensitivity factors for peak to peak heights[16] and correction for the copper interference on the nickel peak (equation 11). Since

$$Wcp = Wcu + Wni + Wo \qquad (16)$$

and we may calculate Wo by either of the two methods previously described, it is necessary only to solve for Wcu or Wni as the other may be calculated by difference.

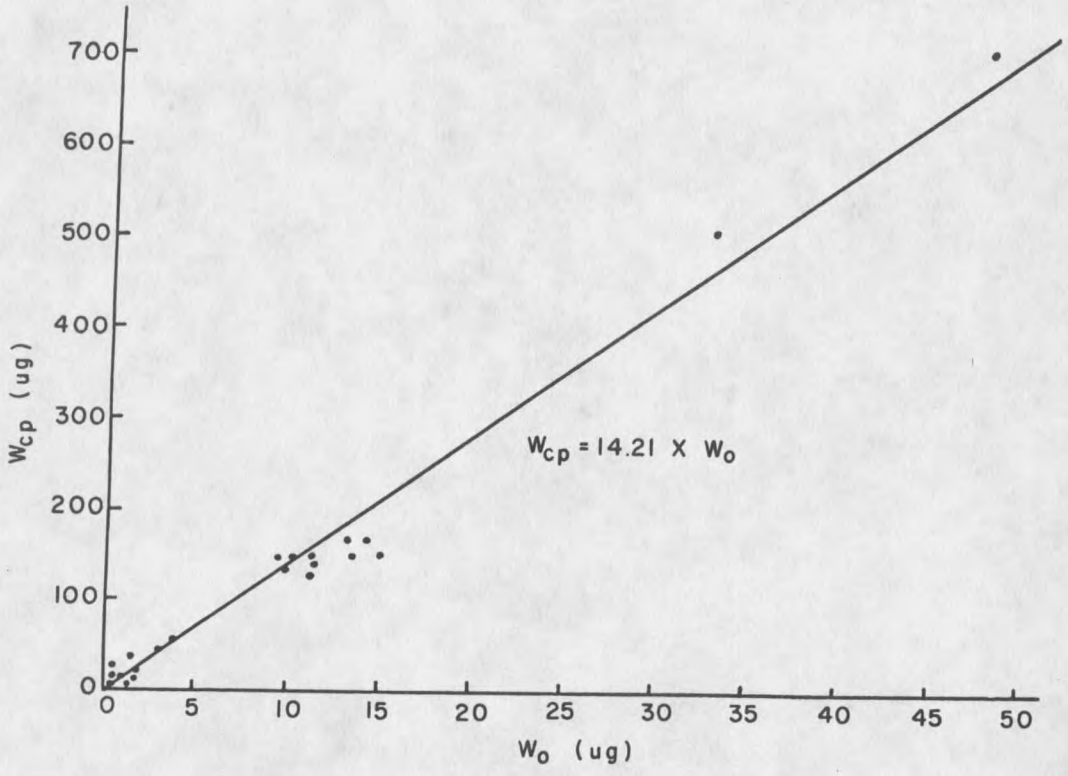


Figure 19. Relationship Between Wo and Wcp.[50]

The ratio of weights of copper to nickel in the corrosion product is expressed in terms of the atomic concentration percents and atomic weights in equation (22).

$$\frac{Wcu}{Wni} = \frac{Capc}{Napc} \times \frac{63.54}{58.71} \qquad (22)$$

Rearrangment yields:

$$Wni = \frac{Napc}{Capc} \times \frac{58.71}{63.54} Wcu \qquad (23)$$

Substitution into equation (16) and simplification gives:

$$Wcu = \frac{Wcp - Wo}{1 + 0.924 \frac{Napc}{Capc}} \qquad (24)$$

To gain a complete understanding of the corrosion processes it is also necessary to characterize the metals lost to solution. This includes soluble and recoverable metals as well as insoluble or precipitated metals. The total weight of metal lost to solution may be described as:

$$Ws = Wsc + Wsn + Wic + Win \qquad (25)$$

where Wsc and Wsn are the recovered copper and nickel as measured by atomic absorption, and Wic and Win are the weights of insoluble copper and nickel lost to solution.

Ws is determined by the difference in weights of the coupon before and after corrosion, plus the weight of oxygen added in formation of corrosion products.

$$Ws = Wbc - Wac + Wo \qquad (26)$$

As it is possible for selective dissolution of Cu relative to Ni to occur, there is no direct method to determine how much of Ws is due to Cu or Ni. It is therefore necessary to calculate Wic and Win by an independent method.

Utilizing the total alloy weight loss, the total weight of copper and that of nickel can be determined. These totals provide a means of calculating Wic and Win as follows.

Considering Fcu as the fraction of copper in the alloy (0.88); the material balance accounting for corrosion product formation,

copper lost to solution, and other copper losses can be described as:

$$(Wbc - Wf)\ Fcu = Wcu + Wsc + Wic + (Wla + Wlr)Fcu \qquad (27)$$

which upon rearrangement yields:

$$Wic = Fcu\ (Wbc - Wf - Wla - Wlr) - Wcu - Wsc \qquad (28)$$

Substituting equation (13) into (28) we get:

$$Wic = F_{cu}(W_{bc} - Wf - Wac - Waa + Wcp \frac{As}{A} - Wlr) - Wcu - Wsc \qquad (29)$$

and a similar treatment for nickel gives:

$$Win = Fni(W_{bc} - Wf - Wac - Waa + Wcp \frac{As}{A} - W_{lr}) - Wni - Wsn \qquad (30)$$

As a final check for accuracy one may utilize the following equation:

$$Wbc - Wf + Wo = Wcp + Ws \qquad (31)$$

This series of derivations were adapted with several changes and revisions from previous work performed on 70/30 cupro-nickel alloy[50]. The application of these is given in the Results and Discussion section.

Inhibitor Experiments

The organic compounds chosen for study are 2-mercaptobenzothiazole (MBT), 2-mercaptobenzimidazole (MBI), 2-mercaptobenzoxazole (MBO), and 2-mercaptothiazoline (MT), and are shown in Figure 20. All were obtained in reagent grade form from Aldrich Chemical Company, Milwaukee, WS.

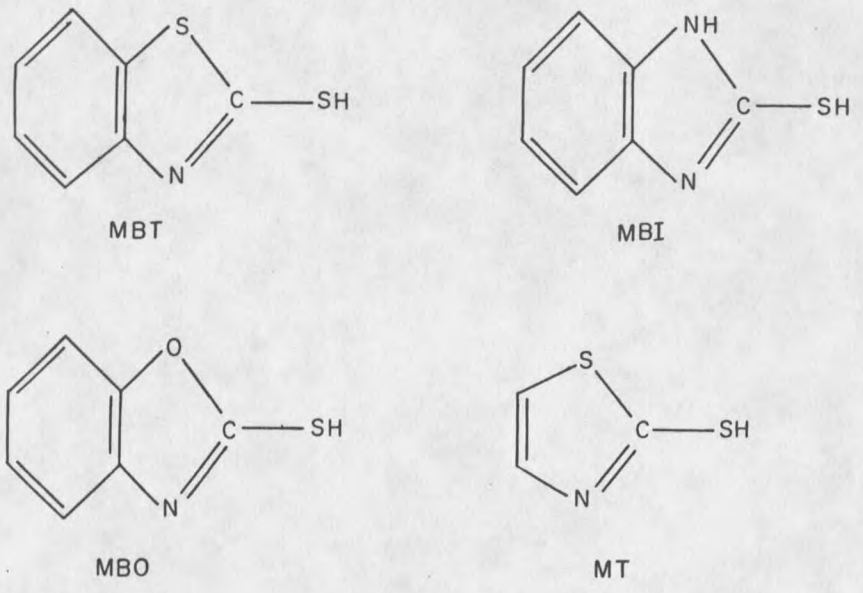


Figure 20. Structures of MBT, MBI, MBO, and MT.

The compounds were tested for inhibition of cupro-nickel alloy corrosion in seawater by two methods. The first method involved dissolving the inhibitor in the seawater solution prior to corrosion testing, and the second method involved pretreating the alloy surface prior to corrosion. The solubilities of the three inhibitors containing a benzene ring were $10^{-3}$ M in seawater, while that of 2-mercaptothiazoline (MT) was greater ($10^{-2}$ M).

Preliminary testing was done over a concentration range of $10^{-3}$ M to $10^{-6}$ M for MBT, MBI and MBO, and from $10^{-2}$ M to $10^{-6}$ M for MT. These tests were run at 30°C, pH = 8, and 1/3 strength artificial seawater for a duration of one hour utilizing the

stirred beaker reactor. The efficiencies of the inhibitors were calculated by comparison to a blank utilizing equation (32).

$$\theta = 1 - \frac{\Delta W}{\Delta Wo} \qquad (32)$$

In this relationship $\theta$ is the inhibition efficiency, $\Delta W$ is the total weight loss with inhibitor present, and $\Delta Wo$ is the total weight loss without inhibitor[57].

A second set of tests with the inhibitors in solution was carried out utilizing the flow reactor and inhibitor concentrations at $10^{-3}$M and $10^{-4}$M. The experimental conditons were T = 30°C; pH = 8, 1/3 strength artificial seawater, and flow at 15 cm/sec. The tests were run for periods of 10 min, 1 hour, 4 hours, 16 hours, and 48 hours for each inhibitor at both concentrations. A blank was run at the same time intervals for comparison purposes, and to calculate inhibition efficiencies.

At certain concentrations some inhibitors produced very thick layers of organic material on the surface which were examined by scanning electron microscopy. In order to measure the overall weight loss during corrosion those bulky layers were removed by ultrasonic agitation in distilled water[58], and the corrosion products removed by a five second dip in 1:1 HCl as discussed previously.

A complete material balance was not utilized in the inhibitor experiments because the organic inhibitors in solution formed films on the Chelex-100 resin and prevented solution analysis. Problems

encountered with organic layers on the coupons during the surface analysis procedures are discussed in a later section.

A third set of tests involved pretreating the coupons by dipping in 60°C distilled water solutions of the inhibitors for two minutes. Copper dipped in 0.25% benzotriazole in water at 60°C for two minutes forms a thin adsorbed or reaction-product film that protects the metal from tarnishing[37]. In the current study a 0.25% solution of MT was used. The other three inhibitors would not dissolve to that extent, so saturated solutions were employed. Samples were corroded for periods of 30 min., 1 hour, 6 hours, 12 hours and 48 hours in the flow reactor under the standard conditions of T = 30°C, pH = 8, 1/3 strength artificial seawater, and flow = 15 cm/sec.

In addition to the weight loss experiments and surface analysis, UV spectra of the inhibitors were taken with a Varian 634 UV-VIS spectrophotometer. The inhibitors were dissolved as 5 x $10^{-5}$ M solutions in 0.1 M $Na_2SO_4$ and the pH was adjusted to 3, 6 and 9 with standard HCl and NaOH in order to investigate spectral changes with pH.

Infra-red spectra were taken of the inhibitors in carbon tetrachloride solutions, and attempts were made to obtain reflection infra-red of the surface films on copper sheet metal. An internal reflectance attachment (R.G. Wilkes, Inc.) was utilized in conjunction with a Nicolet FT-IR but no meaningful data could be obtained. It was determined that reflectance IR data could only be

obtained with mirrored surfaces, and a AgCl[58] or gold wire[59] polarizer, all of which were unavailable.

All weight loss experiments were run in duplicate to ensure good reproducibility. Larger coupons (7 cm long) were also used in an attempt to increase weight changes. Difficulties arose because of flow effects in the reactor with the turbulent conditions employed, and were abandoned in favor of the original design.

# RESULTS AND DISCUSSION

## PRETREATMENT

The depth profile shown in Figure 18 is typical for coupons corroded using the prescribed pretreatment procedure given in the experimental section. The depth profile shows how the atomic concentration percents of copper, nickel, and oxygen vary with depth of penetration of the etching ion beam through the corrosion product layer. Specific information can be derived from these plots concerning the corrosion product tarnish layer:

a) stoichiometry

b) surface coverage

c) layer thickness

d) rate of formation

e) elemental distribution with depth

The stoichiometry of the corrosion product is given by the atomic percent (AT%) level of the plateau of the oxide profile. In this region there is a uniform corrosion product composition with depth which allows estimation of metal to oxygen ratios. Indications of the degree of nickel doping and the composition of the most stable oxide are apparent. The main oxide is associated with copper in a high metal to oxygen ratio, which eliminates CuO as a likely species. The formation of $Cu_2O$ is much more probable

and has been identified as the main protective oxide on cupro-nickel alloys in seawater[60,61].

Other x-ray diffraction and x-ray photoelectron studies of cupro-nickel alloys in seawater[62-64] have determined the presence of dual corrosion product layers, namely an inner protective layer of $Cu_2O$ and an outer porous layer of $Cu_2(OH)_3Cl$. However, the presence of the outer porous layer could not be substantiated in this study. In no case could chlorine be detected even though it is one of the most sensitive elements in the auger analysis[16]. In addition, the presence of an oxide plateau in the depth profiles is consistent with only one corrosion product layer having constant composition with depth. The lack of an outer porous layer can be explained by the approximate once-through conditions of the flow reactor, coupled with relatively short exposure times (<96 hours). These conditions may not allow enough of a concentration buildup of metal ions in solution for precipitation of an outer porous layer of $Cu_2(OH)_3Cl$.

Despite indications of the presence of a protective layer of $Cu_2O$, the depth profile plateaus display a copper to oxygen ratio that is slightly higher than two to one. In fact, the atomic percent data is consistent with an intimate mixture of $NiO:Cu_2O:Cu$ in a ratio of 1:5:7 for the 90/10 alloy as well as the 70/30 alloy[50]. Even if these speciation assignments are not entirely accurate, there is simply too much copper enrichment to consider a pure $Cu_2O$ layer. A lack of detectable anions other than $O^{2-}$ and

the requirement of charge neutrality can only suggest that enriched copper levels are present in reduced form.

A likely source for reduced copper enrichment is the simple equilibrium reaction

$$2\ Cu^{+} \rightleftarrows Cu + Cu^{2+} \qquad (1)$$

which is displaced far to the right[37]. Conceivably, cuprous ions in the oxide layer near the oxide-solution interface can transfer an electron by the above reaction. This would leave reduced copper and a cupric ion near the surface. The divalent ion could then become solvated and diffuse away to the bulk seawater or become complexed with chloride ions and pass to the solution as a soluble complex. In either case, the reduced copper would remain with the $Cu_2O$, producing enrichment without disturbing the charge balance of the corrosion product layer. A competing reaction can occur, namely complexation of cuprous ions from the oxide surface with chloride ions to form soluble $CuCl_x^{1-x}$. Formation of $CuCl_x^{1-x}$, where $x = 2$, could still represent the major dissolution product[37], and the reaction would simply limit the amount of corrosion product left on the metal surface. It should be pointed out that even though this competing reaction could shift the displacement equilibria more to left (equation 1), it is still kinetically feasible for the forward reaction to occur and lead to the observed metal enrichment of the oxide layer. Other factors that apply to this mechanism have been discussed elsewhere[50]. Since information of the type just discussed is necessary for proper evaluation of an alloy's performance, the presence of a plateau in the oxide depth

profile is a major criterion that a pretreatment procedure should meet under the corrosion conditions of this study. The absence of a plateau indicates a non-homogeneous corrosion product layer.

Surface coverage of oxide on a microscopic scale is also indicated by the oxide depth profile. This information can be used to supplement macroscopic observations of patchiness to predict non-reproducibility, excessive roughness, inadequate degreasing, and incomplete removal of surface history. It has been shown by auger element mapping and partial ion beam etching that tarnish layer coverage varies in thickness over the sample surface[50]. A more variable oxide coverage will be indicated by immediate exposure of small areas of clean alloy during etching. The oxide layer will immediately and continually diminish until the last traces of oxygen are removed, without showing a significant plateau in the depth profile. This behavior is usually accompanied by a dull or patchy corroded coupon appearance and poor reproducibility. In contrast, an even oxide coverage will show a well defined reproducible oxide plateau and a uniform, lustrous coupon appearance.

The average thickness of the oxide layer can also be quantified by the oxygen depth profile, provided that a plateau exists. Ideally, a completely uniform oxide coating will produce a block shaped profile where the oxygen concentration immediately drops to zero at the oxide-metal interface. In this case the average thickness would be very easy to determine by the sharp dropoff. The closest approach to the block shape is shown in Figure 18 where the oxide dropoff region is about as wide as the plateau region.

No combination of pretreatment parameters tried would yield a thinner relative dropoff region in a profile. This suggests the limiting shape is controlled by alloy composition-environment interactions and auger instrumental parameters rather than pretreatment. Any further extension of the oxide dropoff rate will have pretreatment procedure dependence which may interfere with interpretation of alloy corrosion properties. Also, the oxide thickness determination will become increasingly difficult and unreliable if the profile gradually diminishes since the average thickness, rather than the last trace of oxide detectable, is desired.

A practical significance of thickness determinations is in the calculation of tarnish rates. However, the pretreatment can complicate thickness determinations, making comparison of tarnish rates difficult. A more useful quantity is derived from the graphical area under the oxide depth profile from the surface to the deepest oxide penetration.

This quantity is independent of profile shape and can be related to the weight of oxide present on the coupon's surface. The area to weight correlation can be made by calculations with oxide lattice parameters, as discussed in the experimental section. A more reliable correlation can be made by direct comparison with oxide weights obtained with a microbalance. The relationship between Wcp and Oa as given in Equations 20 and 21 (Experimental Section) may be utilized to calculate Wcp directly, and the tarnish rate is given by dividing Wcp by the exposure time in minutes.

Comparison of tarnish rates provided another means of evaluating pretreatment procedures. A significantly depressed tarnish rate coupled with a patchy coupon appearance suggested inadequate degreasing where the surface was blocked by contaminants. In general, a higher tarnish rate and a plateau in the depth profile is a good indication of a clean and well prepared surface.

The goal was to develop a pretreatment procedure yielding a reproducible profile with a high tarnish rate and sharp plateau shape. Specific effects of each pretreatment parameter were evaluated based on these criteria.

Roughness

The ASTM Standard Practice g1-81 for preparing, cleaning, and evaluating corrosion test specimens recommends abrading a metal surface with an appropriate abrasive or abrasive slurry[32]. Although no specific grit sizes are suggested for copper and copper alloys, it was assumed those available commercially would suffice. SiC emery paper of 80, 180, 240, 320, 400, 600, and 1200 grit sizes, as well as $Al_2O_3$ polishing paper (~5000 grit) were utilized. These were chosen to cover a wide range in roughness. It should be noted that most new tubing surfaces are at the smooth end of the scale (above 600 grit sizes), so smaller size grits are recommended to better approximate commercial surface roughness.

After abrasion with the appropriate grit emery paper, samples were degreased in acetone and dried under $N_2$ before corrosion. The

auger analyses were performed and the depth profiles were studied for shape and area under the oxide curve. With an increase in roughness it was noted that the plateau as in Figure 18 changed to an immediate linear decrease from the surface to the bottom of the tarnish layer. This was seen with all the rougher grits (320, 240, 180, 80). Micrographs of surfaces that exhibited the linear depth profile shape revealed a nodular three dimensional oxide growth morphology. This is in contrast to the two dimensional surface covering morphology associated with oxide depth profiles that exhibit a plateau. Nodular growth is consistent with a dissolution-precipitation mechanism that is dominated by nucleation and crystal growth. This is in contrast to a smooth and uniform tarnish layer consistent with a solid-state growth mechanism[65].

Nodules appear as separate entities with areas of uncorroded or slightly corroded alloy between them. An immediate and constant decrease in the oxide level occurs as nodules of varying size are removed during sputter etching of these types of tarnish layers. Dobb et al. have provided a complete discussion of nodule formation[66,67].

Since nodule coverage is not expected to be as protective as layer coverage, rougher surfaces should be avoided from a practical point of view. Also, nodular growth is too dependent on flow conditons to allow proper assessment of alloy composition and tarnishing behavior trends. For these reasons, the use of grits larger than 320 should be avoided.

Several problems exist that discourage the use of very smooth grit polishing papers. The first involves a smearing phenomenon that occurs when roughness elements lose mechanical strength as they get smaller[68]. Ridges are smeared and metal is deposited in smears across the surface. Since the deposited metal is highly deformed and may not retain the metal crystal structure, the corrosion behavior is expected to be different than for a fresh metal surface. Pickling the surface by short term (<5 sec) exposure to concentrated $HNO_3$ will remove some of the deposited metal, but may be insufficient to remove a larger quantity. Longer exposure to $HNO_3$ will remove more metal, but pitting and etching will also occur which greatly increases the roughness. Evidence of extensive smearing is seen with grit numbers in excess of 600 whereby residue buildup on the abrasive paper is clearly visible.

Another problem lies in the vigorous strokes required to produce a smooth finish with the finer grits. Such conditions can work-harden the surface and affect the corrosion behavior. Since ASTM[32] cautions against steps that cause work-hardening, the use of finer grits is discouraged.

Figure 21 shows the tarnishing rate behavior versus roughness. The tarnishing rate in $\mu g\ cm^{-2}\ min^{-1}$ was determined by microbalance weighings before and after corrosion product removal in 1:1 HCl, and the grit sizes were converted to scratch widths in microns as determined from micrographs of coupon surfaces[50].

The recommended roughness is given by use of 600 grit SiC paper and corresponds very near to the maxima in the curve shown

in Figure 21. The decrease in tarnish rate for very smooth coupons is due to smearing and/or work-hardening. This problem is minimal at 600 grit, however, a pickling step to remove any smeared metal is still recommended. Coupons abraded with grit sizes rougher than 600 also show decreased reactivity. This behavior is due to nodule formation which exhibits slower growth kinetics and a nucleation induction period that can last up to one hour after the corrosion test is begun.

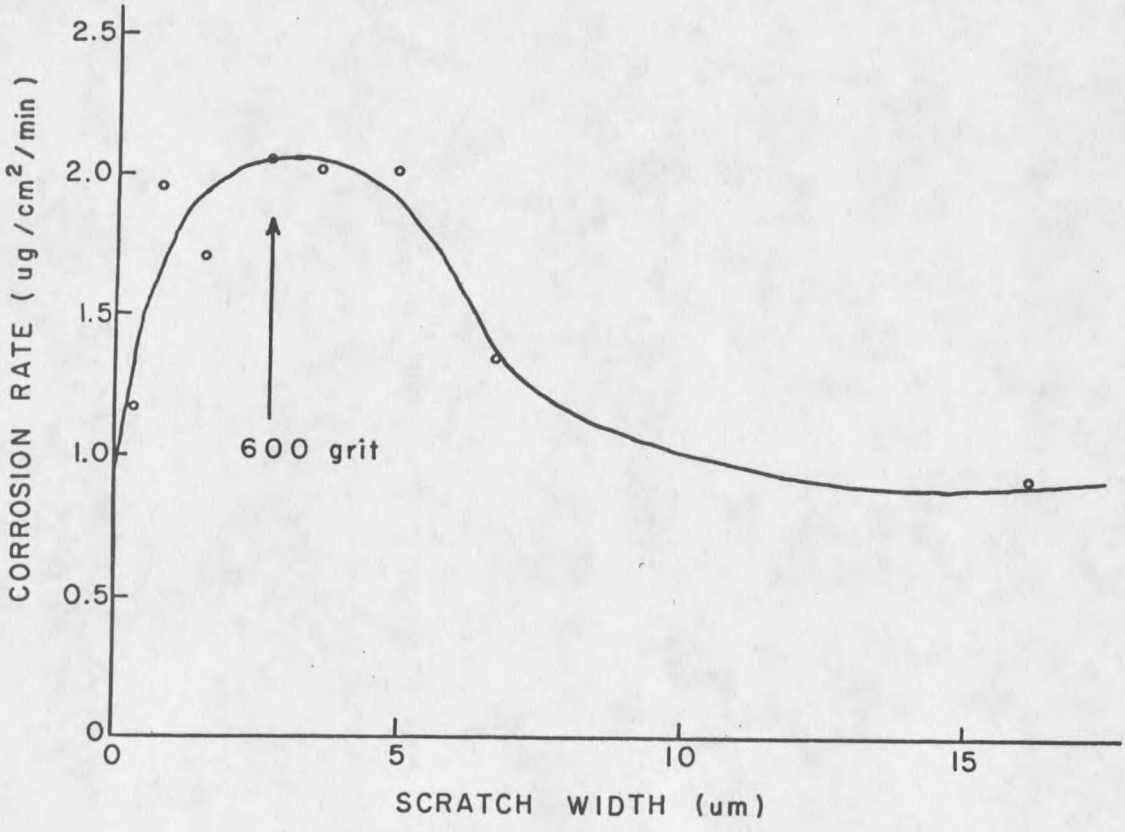


Figure 21. Effects of Surface Roughness on the Corrosion Rate.

Degreasing

ASTM recommends degreasing in an organic solvent or hot

alkaline cleaner with or without ultrasonic cleaning to remove machine oil and debris from the alloy manufacture and sample handling[32]. Surface contaminations affect the tarnish rate as well as reproducibility, hence some step is necessary for removal. Also the auger analysis requires an ultra high vacuum which is adversely affected by volatile organic compounds.

Three organic solvents were tested: acetone, methanol, and carbon tetrachloride. Acetone was found to allow the greatest reactivity and is the recommended solvent for organic degreasing[29]. It is felt that the organic degreasing step may provide a more uniform surface for the acid pickling step which follows.

Acid Pickling

The recommendation of ASTM[32] is to pickle copper and cupro-nickel alloys in 50% HCl or 10% $H_2SO_4$ for one to three minutes prior to corrosion testing. Preliminary testing on the 70/30 alloy[29] showed an uneven tarnish layer and poor reproducibility with these acids, whereas concentrated $HNO_3$ was found to be effective as an acid pickling agent.

Although the concentrated $HNO_3$ worked well for the 70/30 alloy, a 5 second dip in concentrated $HNO_3$ resulted in excessive roughness and pitting with the 90/10 alloy. After testing the two alloys in a range of concentrations of $HNO_3$ from 5% to concentrated, it was found that a 5 second dip in 25% $HNO_3$ provided the most uniform surface and reproducible results for both alloys, and is the recommended pickling agent[29].

Sample Storage

Cleaned coupons left open to the atmosphere will develop a tarnish layer quickly, making some form of sample storage necessary. Coupons stored in small dessication vials over $CaCl_2$ and under $N_2$ showed no variation in analyses over a six month time period. Also cleaned coupons stored in this manner showed no detectable oxide layers forming over the same time period. It is felt, therefore, that this method of sample storage is satisfactory.

Pretreatment Summary

The recommended pretreatment procedure, as described in the experimental section, gives a clean and reproducible surface. The surface is representative of the bulk alloy and assures that tarnishing behavior is only a function of alloy composition.

The pretreatment parameters exhibiting the greatest effect on subsequent short term corrosion behavior of cupro-nickel alloys in seawater were determined to be surface roughness and acid pickling. Degreasing was found to have less influence on the corrosion behavior, but can significantly affect reproducibility. Sample storage in individual $CaCl_2$ dessication vials under $N_2$ was found to be satisfactory.

## MATERIAL BALANCE

The data for the mass balance analyses are given in Tables 7-11. Table 7 describes the conditions of each experiment or run, and how they differ from the base conditions given previously (1/3 strength salinity, saturated dissolved $O_2$, pH = 8.0, T = 30°C, flow = 15 cm/sec, and 30 minutes exposure time). Table 8 is the raw mass balance data, microbalance weights and the oxide area calculated from the depth profiles. The data in Table 9 include the calculated atomic concentration percents of elements in the oxide layer, the calculated weight of corrosion product deposited on the coupon, and the elemental composition of the corrosion product. Solution losses, both recoverable and insoluble, are listed in Table 10.

To evaluate trends in the corrosion processes and to show how different parameters effect these processes, Table 11 was constructed. The (Wcp-Wo)/Ws column compares the metal in the corrosion product to the metal lost to solution. If this ratio is high, the corrosion process results primarily in formation of a protective layer on the coupon and is desirable from a corrosion prevention point of view. If the ratio is low, alloy dissolution is favored.

TABLE 7. Material Balance Data Set 1.

| Run | Parameter | Value |
|---|---|---|
| 1 | Base | * |
| 2 | Time | 6 hr. |
| 3 | | 12 hr. |
| 4 | | 24 hr. |
| 5 | | 48 hr. |
| 6 | Temperature | 5°C |
| 7 | | 10°C |
| 8 | | 20°C |
| 9 | | 30°C |
| 10 | | 40°C |
| 11 | Salinity | 2 g/kg |
| 12 | | 5 g/kg |
| 13 | | 10 g/kg |
| 14 | | 20 g/kg |
| 15 | | 30 g/kg |
| 16 | Dissolved $O_2$ | 0.4 ppm |
| 17 | | 0.7 ppm |
| 18 | | 1.4 ppm |
| 19 | | 4.0 ppm |

*30 min, 30°C, 10 g/kg salinity, 7.5 ppm dissolved $O_2$

TABLE 8. Material Balance Data Set 2.

| Run | Wbc (g) | Wac (g) | Waa (g) | Wf (g) | Oa (AT%·Å) |
|---|---|---|---|---|---|
| 1 | 1.4718160 | 1.4717907 | 1.4718027 | 1.4716540 | 7,392 |
| 2 | 1.5810823 | 1.5810006 | 1.5809837 | 1.5805273 | 8,850 |
| 3 | 1.5095133 | 1.5093030 | 1.5092850 | 1.5087157 | 12,168 |
| 4 | 1.3784603 | 1.3780813 | 1.3780433 | 1.3774333 | 19,062 |
| 5 | 1.3469847 | 1.3460967 | 1.3460873 | 1.3455417 | 20,022 |
| 6 | 1.2975240 | 1.2975057 | 1.2975040 | 1.2974433 | 3,549 |
| 7 | 1.3515373 | 1.3515097 | 1.3515333 | 1.3514517 | 3,870 |
| 8 | 1.3086973 | 1.3086860 | 1.3086743 | 1.3085727 | 6,900 |
| 9 | 1.4273287 | 1.4273167 | 1.4273073 | 1.4271917 | 6,654 |
| 10 | 1.3455380 | 1.3455097 | 1.3455150 | 1.3453713 | 7,011 |
| 11 | 1.4031750 | 1.4031517 | 1.4031793 | 1.4030910 | 2,871 |
| 12 | 1.3439247 | 1.3439143 | 1.3439257 | 1.3438033 | 3,510 |
| 13 | 1.4718160 | 1.4717907 | 1.4718027 | 1.4716540 | 7,392 |
| 14 | 1.3862420 | 1.3861777 | 1.3861773 | 1.3861463 | 2,904 |
| 15 | 1.3477667 | 1.3477333 | 1.3477420 | 1.3477197 | 21 |
| 16 | 1.3830257 | 1.3830293 | 1.3830260 | 1.3829730 | 2,439 |
| 17 | 1.2945980 | 1.2946186 | 1.2946150 | 1.2945637 | 5,532 |
| 18 | 1.3487853 | 1.3487540 | 1.3487563 | 1.3486850 | 6,585 |
| 19 | 1.3462363 | 1.3462280 | 1.3462287 | 1.3460850 | 13,373 |

TABLE 9. Material Balance Data Set 3

| Run | Capc (%) | Napc (%) | Oapc (%) | Wcp (µg) | Wcu (µg) | Wni (µg) | Wo (µg) |
|---|---|---|---|---|---|---|---|
| 1 | 75.4 | 3.3 | 21.3 | 150.1 | 138.1 | 5.6 | 6.4 |
| 2 | 68.0 | 10.9 | 21.1 | 462.8 | 396.5 | 58.7 | 7.6 |
| 3 | 73.5 | 6.1 | 20.4 | 577.5 | 526.6 | 40.4 | 10.5 |
| 4 | 68.1 | 11.1 | 20.8 | 618.9 | 523.6 | 79.0 | 16.4 |
| 5 | 67.6 | 12.8 | 19.6 | 553.5 | 456.4 | 79.8 | 17.3 |
| 6 | 73.5 | 9.3 | 17.2 | 60.7 | 51.6 | 6.0 | 3.1 |
| 7 | 78.3 | 2.5 | 19.2 | 81.9 | 76.3 | 2.3 | 3.3 |
| 8 | 68.4 | 10.0 | 21.6 | 102.2 | 84.8 | 11.4 | 6.0 |
| 9 | 74.4 | 5.0 | 20.6 | 116.5 | 104.3 | 6.5 | 5.7 |
| 10 | 68.4 | 10.6 | 21.0 | 145.0 | 121.6 | 17.4 | 6.0 |
| 11 | 76.5 | 9.1 | 14.4 | 88.7 | 77.7 | 8.5 | 2.5 |
| 12 | 69.7 | 12.0 | 18.3 | 123.4 | 103.9 | 16.5 | 3.0 |
| 13 | 75.4 | 3.3 | 21.3 | 150.1 | 138.1 | 5.6 | 6.4 |
| 14 | 76.0 | 10.1 | 13.9 | 30.5 | 25.0 | 3.0 | 2.5 |
| 15 | 88.2 | 9.3 | 2.5 | 21.6 | 19.7 | 1.9 | <0.1 |
| 16 | 78.8 | 2.6 | 18.6 | 52.8 | 49.2 | 1.5 | 2.1 |
| 17 | 68.2 | 12.7 | 19.1 | 51.1 | 39.5 | 6.8 | 4.8 |
| 18 | 70.9 | 9.1 | 20.0 | 71.4 | 53.6 | 6.4 | 11.4 |
| 19 | 71.0 | 8.1 | 20.9 | 145.0 | 116.4 | 12.3 | 16.3 |

TABLE 10. Material Balance Data Set 4.

| Run | Ws (µg) | Wsc (µg) | Wsn (µg) | Wic (µg) | Win (µg) |
|---|---|---|---|---|---|
| 1 | 31.7 | 18.0 | 15.0 | 1.8 | - |
| 2 | 89.3 | 85.0 | 42.3 | 8.6 | - |
| 3 | 220.8 | 98.0 | 52.5 | 85.1 | - |
| 4 | 395.4 | 128.0 | 61.8 | 246.5 | - |
| 5 | 905.3 | 220.0 | 86.4 | 620.9 | - |
| 6 | 21.4 | 10.1 | 5.8 | 9.4 | - |
| 7 | 30.9 | 17.0 | 7.1 | 5.3 | 1.6 |
| 8 | 17.3 | 13.7 | 8.5 | 3.7 | - |
| 9 | 17.7 | 20.4 | 12.0 | - | - |
| 10 | 34.3 | 26.5 | 12.3 | 7.9 | - |
| 11 | 25.8 | 5.0 | 7.0 | 18.1 | - |
| 12 | 13.4 | 10.0 | 10.0 | 6.5 | - |
| 13 | 31.7 | 18.0 | 15.0 | 1.8 | - |
| 14 | 66.8 | 63.0 | 12.0 | - | - |
| 15 | 33.4 | 27.0 | 10.0 | 2.8 | - |
| 16 | 7.5 | 4.0 | 3.5 | - | 0.1 |
| 17 | 10.5 | 6.5 | 4.0 | - | - |
| 18 | 42.7 | 11.0 | 6.5 | 25.8 | - |
| 19 | 24.6 | 17.0 | 12.0 | 1.5 | - |

TABLE 11. Material Balance Data Set 5

| Run | Wcp-Wo / Ws | Wcu/Wni | Wsc/Wsn | Wcu/Wsc | Wni/Wsn | Wbc-Wf (ug) |
|---|---|---|---|---|---|---|
| 1 | 4.53 | 24.7 | 1.20 | 7.67 | 0.37 | 162 |
| 2 | 5.10 | 6.75 | 2.01 | 4.66 | 1.39 | 555 |
| 3 | 2.57 | 13.0 | 1.87 | 5.37 | 0.77 | 798 |
| 4 | 1.52 | 6.63 | 2.07 | 4.09 | 1.28 | 1027 |
| 5 | 0.59 | 5.72 | 2.55 | 2.07 | 0.92 | 1443 |
| 6 | 2.69 | 8.60 | 1.74 | 5.11 | 1.03 | 81 |
| 7 | 2.54 | 33.2 | 2.39 | 4.49 | 0.32 | 86 |
| 8 | 5.56 | 7.44 | 1.61 | 6.19 | 1.34 | 125 |
| 9 | 6.25 | 16.1 | 1.70 | 5.11 | 0.54 | 137 |
| 10 | 4.05 | 6.99 | 2.15 | 4.59 | 1.41 | 167 |
| 11 | 3.34 | 9.14 | 0.71 | 15.5 | 1.21 | 84 |
| 12 | 8.99 | 6.30 | 1.00 | 10.4 | 1.65 | 121 |
| 13 | 4.53 | 24.7 | 1.20 | 7.67 | 0.37 | 162 |
| 14 | 0.42 | 8.33 | 5.25 | 0.40 | 0.25 | 96 |
| 15 | 0.64 | 10.4 | 2.70 | 0.73 | 0.19 | 47 |
| 16 | 6.76 | 32.8 | 1.14 | 12.3 | 0.43 | 53 |
| 17 | 4.40 | 5.81 | 1.63 | 6.08 | 1.70 | 34 |
| 18 | 1.41 | 8.38 | 1.69 | 4.87 | 0.98 | 100 |
| 19 | 5.23 | 9.46 | 1.42 | 6.85 | 1.03 | 151 |

The Wcu/Wni column compares the copper to nickel ratios in the corrosion product layer, and is a measure of the Ni incorporation into the $Cu_2O$ lattice. With higher Ni, the electrical and ionic resistivity of the oxide layer increases, resulting in increased passivity. For the 90/10 alloy there is considerable uncertainty as very small changes in the Ni will result in large deviations in Wcu/Wni ratio.

The Wsc/Wsn column compares the metals lost to solution, and the relatively low values suggest Ni is preferentially dissolved with respect to Cu (if simple alloy dissolution were occuring one would expect the ratio to be around 9 for 90/10 cupro-nickel alloy). Thus copper is preferentially retained in corrosion product formation.

The ratios Wcu/Wsc and Wni/Wsn compare the Cu and Ni in the corrosion product to their losses to solution. A high ratio of Wcu/Wsc is desirable as initial corrosion results in protective layer formation. These columns represent the breakdown of (Wcp-Wo)/Ws into the individual alloying components and the conclusions which can be drawn are similar.

The last column (Wbc-Wf) gives the total weight of the alloy involved both in corrosion product formation and solution loss. This term is utilized as a measure of the total corrosion rate, and is the factor utilized determining which conditions result in increased corrosion.

Exposure

A primary reason for studying short term corrosion behavior of an alloy is to ascertain how a protective layer forms. The tarnish layer is critical in helping the alloy resist chemical attack, and if it has the ability to reform when penetrated, the alloy will be protected. Tarnishing is detectable by auger analysis and visually during the first hour of exposure to seawater. The color changes through light yellow, brown, purple, blue, and blue-green during this time period. Gradually the surface finish is dulled, and takes on a grey color after two days of exposure.

Figure 22 shows how total alloy weight loss varies with exposure time. In the initial phase the alloy loss is high due to solution losses as well as the formation of protective oxide. As the oxide layer increases in thickness the rate of alloy weight loss significantly decreases. Eventually this approaches a steady state condition where the rate of continued growth of the oxide layer is the same as the rate of oxide dissolution. This is evidenced by the leveling off of the curve and is supported by other experiments ranging in duration up to 96 hours. The auger depth profiles of coupons corroded 96 hours showed oxide layers approximately 2000 Å thick. Some enrichment of NiO in the $Cu_2O$ lattice was also evidenced in coupons corroded for the longer exposure times. This shows that a reorganization in the oxide layer is occuring.

Tarnish growth during the first hour is rapid and essentially linear with time. Previous studies[69,70] have shown linear tarnish

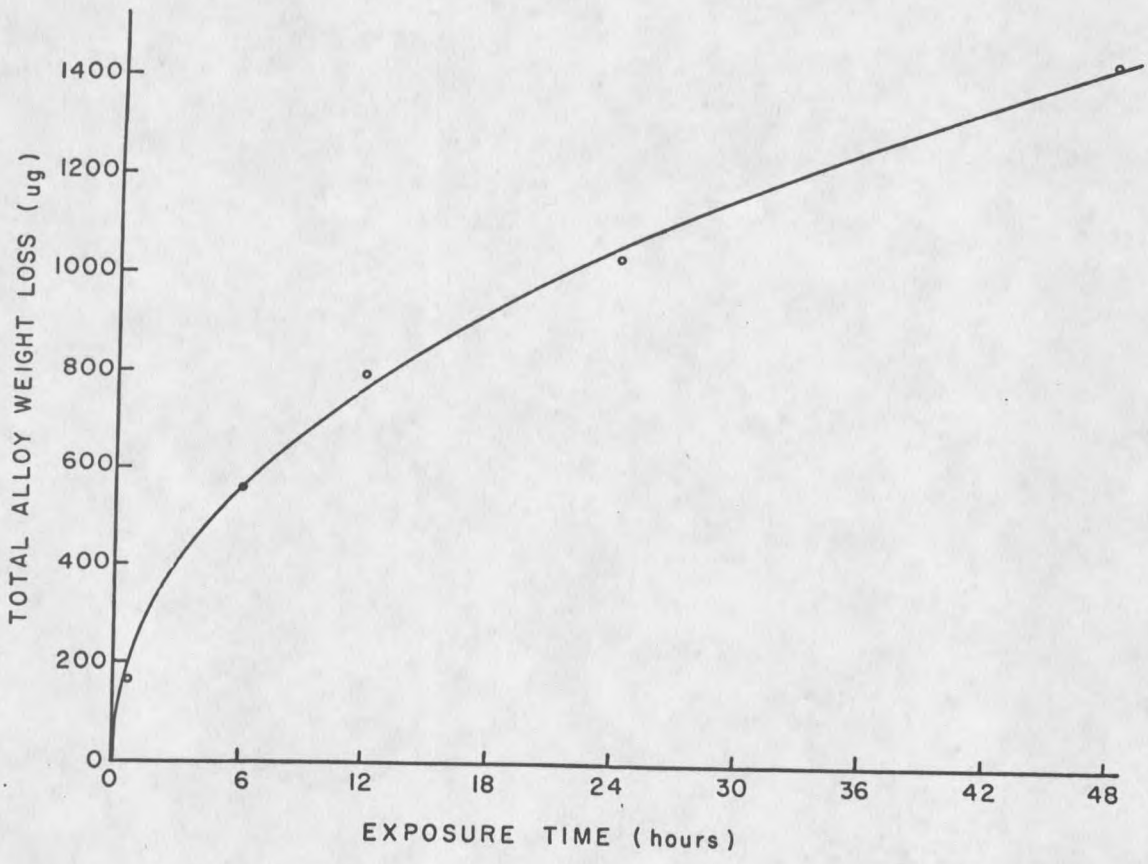


Figure 22. Dependence of Total Alloy Weight Loss on Exposure.

behavior to be evidence for a porous and nonprotective film, but the actual coverage for 90/10 CuNi alloy during short exposure times is quite uniform, as evidenced by scanning electron microscopy in Figure 23. Fractures in the oxide will also result in linear tarnishing with time, as described by Pilling and Bedworth[71]. There is no evidence for a nonprotective film forming, but during early growth stages migration through the relatively thin oxide layer is probable.

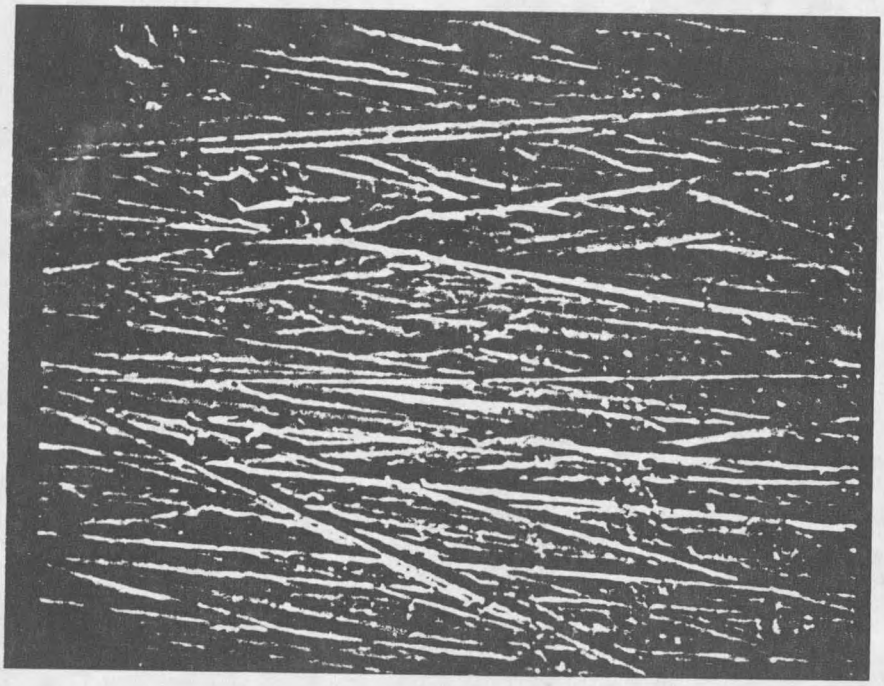

Figure 23. Micrograph of Coupon Corroded Under Base Conditions (1000X).

A criterion for protective oxide formation is the volume increase of the oxide formation relative to the metal[69,70]. When the oxide of a metal occupies too small a volume pores and fractures will form. If the oxide occupies too large a volume, fractures and buckling occurs. $Cu_2O$ is in between the two cases and forms a tightly packed and protective tarnish layer.

At the flow rate utilized in this study, diffusion control and concentration polarization can determine the corrosion rate[50]. Cathodic polarization is evidenced and the linear growth of the oxide layer results from diffusion of $OH^-$ away from the surface. This is independent of the thickness of the oxide layer during early stages.